Acta
Technica
Jaurinensis

Vol. 11, No. 2, pp. 44-60, 2018
DOI: 10.14513/actatechjaur.v11.n2.443
Available online at acta.sze.hu

Architectural and Structural Design of Free-form Structures – Case Study

K. Károlyfi[1], G. László[2], F. Papp[3], R. Bükkösi[4]

[1,2,3,4]Széchenyi István University, Dep. of Structural and Geotechnical Engineering
Egyetem tér 1., 9026, Győr, Hungary
e-mail: [1]k.kitti93@gmail.com, [2]ygab17@gmail.com, [3]pappfe@sze.hu, [4]raymond.bukkosi@gmail.com

Abstract: This article describes the conceptual design process of an equestrian centre, presenting the covered stadium of the building complex in detail, designed it as a free-form, wide-span steel structure. The main goal of this study is to present the application of the parametric design method through a case study and to examine the interoperability opportunities between architectural and structural design software.

Keywords: free-form, parametric design, wide span, steel structure

1. Introduction

Recently thanks to the development of the software aided designing and manufacturing technologies the opportunities of architects significantly increased. This makes it possible to design and accomplish double curved constructions with complex geometry. Free-form edifices exist since the ‘50s but in the last decades their number is increased. Architectural proceeding was a stylistic issue until the second half of the 20th century, buildings denotes the marks of the relevant architectural styles. In our days there is a considerable changing: now the presence of a building is defined by an architectural concept not by the style of the era. As a consequence architects can select from various construction tools, thus they use free forms more often nowadays.

Designing a free form edifice is a complex process demanding particular accuracy. For a satisfying consequence in the case of such an edifice a very close collaboration is indispensable from the beginning of the conceptual designing between the architect and the structural engineer. In case of these buildings the

function, the structure and the form influences each other firmly, thus it is important that both professions have to do with the other in some measure. [1]

The aim of the project presented in this paper is to examine the applicability of parametric design method through a case study, including both of architectural and structural conceptual design. Furthermore, the examination of the interoperability opportunities of structural and architectural design software have a decisive role in this study. The design task was inspired by the vision of the Olympics in Budapest in 2024, which gave a chance to design a representative, great volume facility – an equestrian centre.

2. Architectural design concept

According to the feasibility study published by the Hungarian Olympic Committee [2], the equestrian sport has shown an appreciable demand for a new facility out of the Olympic sports. Additionally, the jumping competitions and dressage tests become increasingly popular in the world, however in eastern-Europe there is not any equestrian venue, that is capable for international and world competitions. Furthermore, the equestrian sport has considerable tradition in Hungary, which is worthy for revival. Based on the feasibility study the building complex was designed near the Olympic Village, on a large and calm green island of the Danube River, the so-called Csepel-Island.

2.1. Design program

The design objective was to create a representative facility, which utilizes the possibility given by the architecture of the 21st century and represents the dynamism and power of the equestrian sport by the form and used architectural tools. The main consideration of the architectural concept was the use of the free-form and parametric design method. The building complex should resuscitate the tradition with the tools of the modern architecture. The chosen area will not detain free-form designing and there is no any assimilation difficulty. In the course of design the coherent forms, emblematic appearance was a very important point, since the building complex should identify as an Olympic venue too.

The equestrian centre has functionally two objectives. On the one hand it ensures indoor and outdoor sport facilities including the theoretical and practical education both in hobby and competition level, the horse therapy and the boarding services [3]. On the other hand it offers recreation possibility for the viewers by giving place for domestic, international and world competitions and other sport and cultural events. To satisfy the defined demands the building complex consists covered and uncovered racecourses with adequate seating capacity, as well as covered and uncovered warm-up courses connected directly to the racecourses.

The main approach of the building complex is in the north, while the service road leads from the western street to the south-west side of the centre. The layout of the two stadiums is acute-angled, therefore the entrance hall between them flares out and so allures the guest. The warm-up halls are encompassed by an articular hill in order to keep coherent formatting. On the southern side of the composition the stables and storages are located following the lines of the composition and closing it. (Fig. 1.)

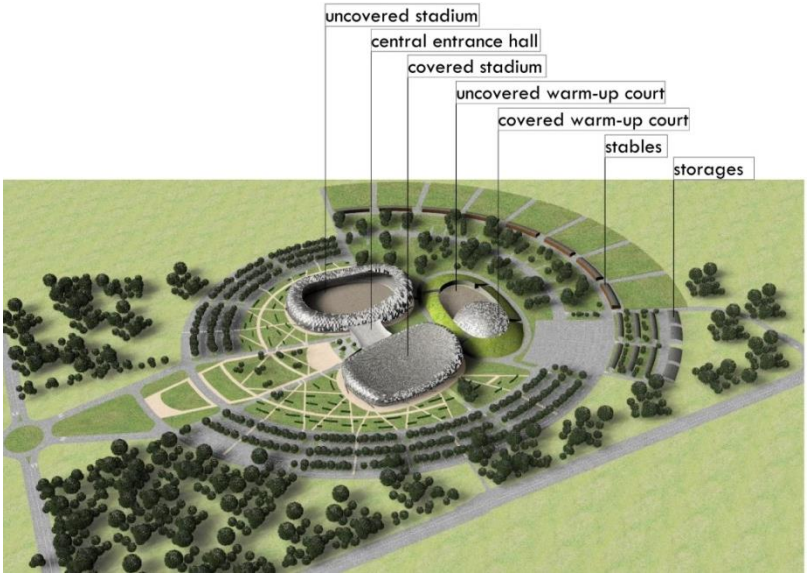

Figure 1. The building complex

2.2. Design of the covered stadium

The size of the racecourse in the covered stadium meets the requirements of the International Federation of Equestrian Sports [4, 5] and exceeds it (40x80 m) in order to use it multifunctional. Therefore the overall dimension of the building is 136x100 m and has a seating capacity of 4500 guests. In the building there are private spaces – viewing area, buffet, and restaurant – for the umpires, the rooms for the media and the VIP guests, offices, general engineering room and changing rooms for the equestrians. These rooms may locate centred, in one compact mass paying attention to adequate visibility of the racecourse.

2.3. Form finding

In the case of the covered stadium the form came mainly from the function. A significant mass – a four-storey reinforced concrete building part – will be resulted by locating the above mentioned centred. According to larger height demand of the auditorium a translation surface, the hyperbolic paraboloid was used for the main form of the stadium. Because of the higher reinforced concrete building part the parabola was deformed on the southern side. The building form as an emblematic saddle is in accordance with the demands described in design program (Fig.2).

Figure 2. The form of the stadium

3. Parametric design process

For modelling this double-curved surface, parametric design method was used. The main advantage of this method is that the form and dimensions can be easily modified later on. Additionally, it is also easier to create and join organic shapes. This flexibility is a fundamental aspect in any design activity, where the designer is constantly going forward and backwards, in order to develop the optimal solution. Using this powerful method, the architectural forms and structural solutions can be designed in an easy and interactive way. [6] In this study the Rhinoceros 3D design software [7] was used with a plug in called Grasshopper. [8] The modelling method is demonstrated here through the implementation of the saddle-shaped surface of the covering shell. The curve of the cross-section was run over the hyperbolic cosine function according to the curve of the longitudinal section. (Fig.3)

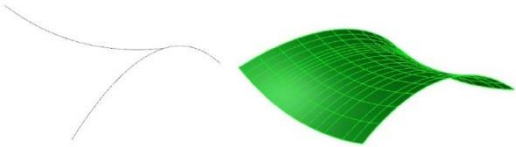

Figure 3. Constructing the saddle-surface [9]

The position of the points of this curve is variable with a help of each parameters, therefore the whole surface is flexible (Fig. 4.).

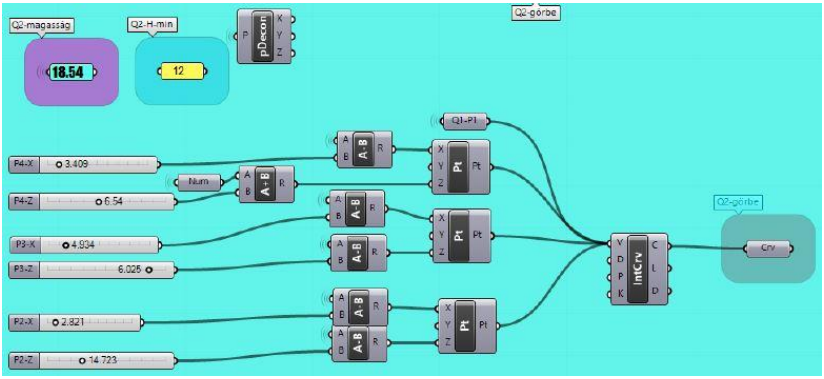

Figure 4. The command box of a main curve of the sidewall surface (Grasshopper) [9]

The whole building structure – including the steel grid and other structural elements – was elaborated using this method. During the conceptual design process it has seen to be an effective tool; the height and dimensions of the structural elements had to be constantly modified in order to reach an optimal solution in both of architectural and structural point of view.

3.1. Grid generation

After implementation of the main architectural form, the next step was the grid generation. In the case of the equestrian centre basically a triangular grid was applied in accordance with the aesthetic and economical aspects. Quadrangle-meshed nets can also be used on double-curved surfaces, but usually the quadrangles of the surface are not planar, which can enhance the costs of the facing material. [10] Two types of triangular meshes were constructed for the surface. (Fig.5) The parametric design method provides facilities for examination of these nets: the number of nodes, the distribution of the elements in certain range of length may be demonstrated, minimal and maximal lengths of elements can be examined. Based on these examinations the second grid was shown more favourable because of the less number of elements and less number of elements of different-lengths, which is advantageous from the point of view of production. Additionally, the aesthetic appearance of the second mesh was an influential factor. Using this variant of net the composition and the rhythm of the covered and glassed triangles may be various, and the architectural formatting may be exciting.

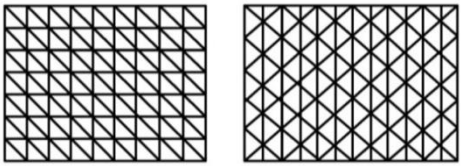

Figure 5. Examined triangular meshes [9]

The generation method of the grid consists of two parts in the case of the stadium: the mesh of the sidewall surface and the saddle surface. First the sidewall surface is described. Dividing the ground-plan curve into defined (and variable) number of equal parts, curves of the triangular mesh located in the vertical plane – with the main curves parallel – can be obtained. After that, dividing these "vertical" curves further, the diagonal curves can be also created. (Fig. 6)

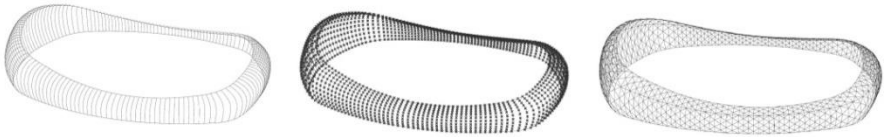

Figure 6. Generation of the mesh of the sidewall surface

The generation method of the mesh of the saddle surface is the projection method, which is a commonly used way in the case of domes. [11] The saddle-surface, in accordance with the sidewall surface was given lamella structured net (Fig.7. a). The basic points of the grid were given by the curves of the sidewall grid joined to the connection line between the sidewall and the saddle-surface. Running the lines into the centre of the surface (Fig.7. b) and dividing into equal parts the concentric curves to the contour of the surface may be obtained. The intersection points of the concentric curves and radial lines were resulted in the nodes. Because of the dimension of the surface the number of the dividing points was halved twice (Fig.7. c) in order to creating elements of ideal lengths. Grouping the concentric curves into three segments the lamella grid can be created (Fig.7. d), by using connective rings, which transmit the forces.

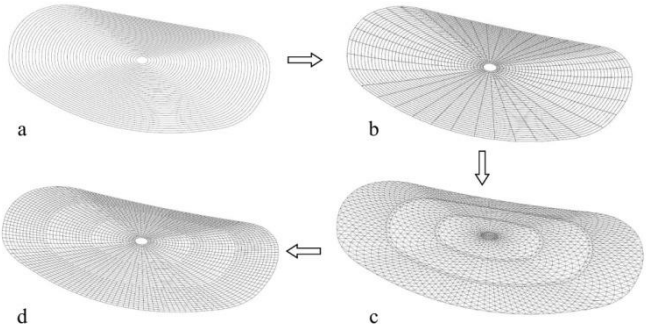

Figure 7. Generation of the grid of the saddle-surface

4. Structural design concept

4.1. Variations

The covering structure is a single-layer triangle meshed steel grid. Because of the function, the building cannot be supported by internal columns however the clearly membrane behaviour is impossible in consequence of the form. Two concepts were invented for the structural performance. The first variety is a hierarchical structural system which consists of a grid surface covering the barrier and a frame-system based on main beams [9]. (Fig. 8) This frame supports the shape of the structural form and bears the reaction forces of the grid surface. Transmission of the forces is ensured by an edge beam between the two elements of the hierarchical system. The second variety owns a similar hierarchy, nevertheless the frame based on main beams is connected directly with the continuous mesh of sidewall and saddle-shaped surface.

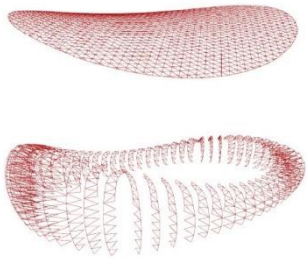

Figure 8. Hierarchical structural concept [9,12]

It was an important goal of the project evolving a concept which is optimal in architectural and also in structural aspect. For this reason several variety of main beamed system was designed and analysed. Essentially two ways of performance were worked out: a clear and simple form and an organic one (Fig.12). Finally, the organic form was applied in the aspect of aesthetics attentive to the influencing factors of the structure. As a consequence of the covering saddle-shaped surface's deflection, a damaging amount of moments and tension forces may be transmitted. To preclude this phenomenon it is recommended to attach the main beams to the covering mesh in the more points and the more orientations as it possible. Furthermore the lever arm can be increased by placing the main beam farther from the joining line of the saddle-shaped surface and the sidewall. Hence to guarantee the structural form the two kind of main beams should be combined. The result of the combination is shown on Fig. 10. It is a frame based on main beams which connect each other and to the mesh around the barrier.

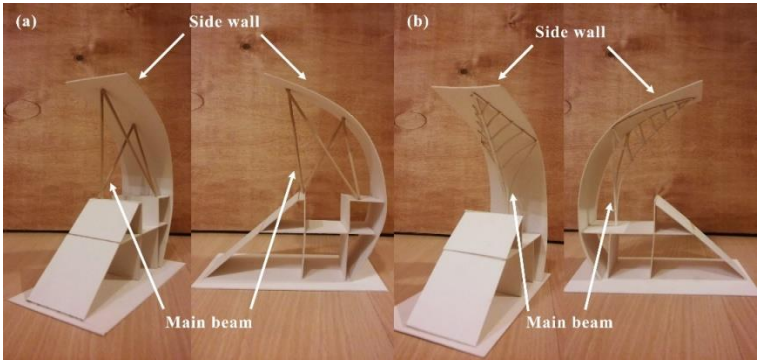

Figure 9. Variations for the main beams

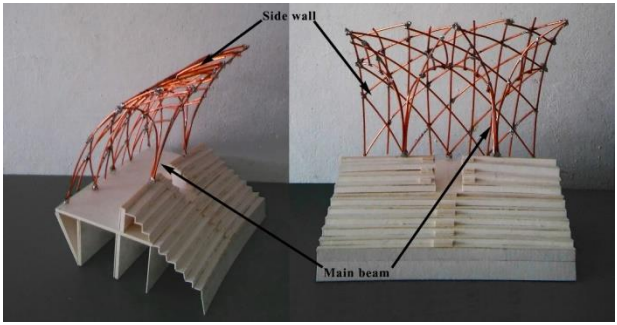

Figure 10. Final version of main beam

4.2. The global structural model

Fig. 11 shows the structural model of the steel construction. Concerning the architectural concept, all bars are made of hot-rolled CHS segments. The bars joined directly with the covering shell are straight and the column members are curved. The conceptual model do not consists the elements of the reinforced concrete substructure, the effect of it is replaced by rigid supports.

Figure 11. Global structural model of the construction: (i) complete model; (ii) supporting columns [12].

The conceptual design of the structure is accomplished for dead load (self weight + sheet: 0,3 kN/m^2) and for the Hungarian one-sided snow load (1,0 kN/m^2) for the sake of simplicity and in the lack of wind-tunnel examination. The global structural behaviour may be approximated by a tensioned chain along the longitudinal axis and a compressed arch along the cross axis of the building (Fig.12).

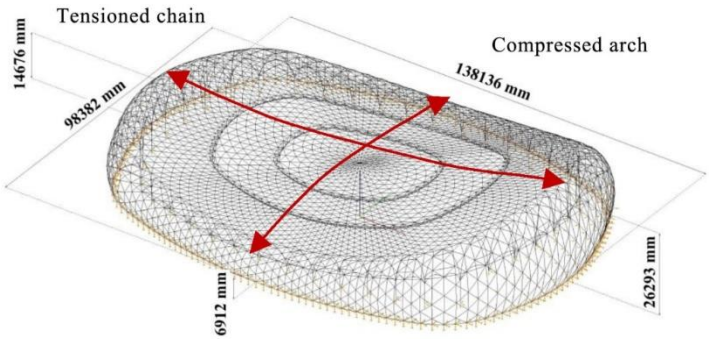

Figure 12. The global force behaviour of the construction [12]

Due to the building's interior design the performance of the grid cannot follow the global force behaviour of the construction. The "frames" constituted by the internal columns and arches and the external central planar bars cannot be rigid enough to strain the surface along or to insure the compressed-arch-like behaviour. At this point, considering the effect of the reinforced concrete substructure became a key-question in the designing. In Fig. 13 the global deformation of the structure

is shown with the substructure's supporting effect. The maximum deflection is 313 mm, which value may be accepted.

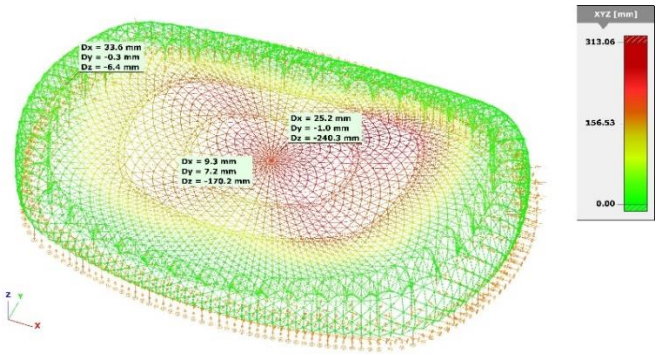

Figure 13. Global deformation of the structure with the supporting effect of the reinforced concrete substructure [12]

4.3. Design of the cross sections

The entire model is divided to ten groups based on by the initial stresses. Bars in each group have identical diameter and thickness of CHS cross-section. Sizes of sections are ranged from CHS 139.7x4 up to CHS 508x20. The largest sections are needed for the vertical bars of the lateral-wall and the bars of the internal columns. Minor sections are used for the internal zones of the saddle-shaped surface. The utilization of cross-sectional resistances according to the EN 1993-1-1 [13] is shown in Fig. 14. The specific structural steel usage of 128 kg/m^2 can be decreased by virtue of particular designing.

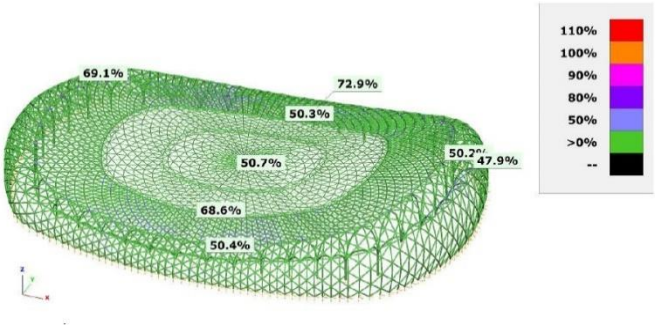

Figure 14. Utilization of resistances of the structure selected in ten groups of sections according to EN 1993-1-1 [12, 13]

4.4. Global stability analysis

The global stability analysis begins with determining the elastic stability loss ways. Typical elastic global buckling modes and critical load multipliers of the structure are shown in Fig. 15. According to the stability loss modes and the critical load multipliers the consequences are the followings:

- the value of the first critical load multiplier (α_{cr}=1.61) is too low
- the buckling shape fluctuates along two concentric rings.

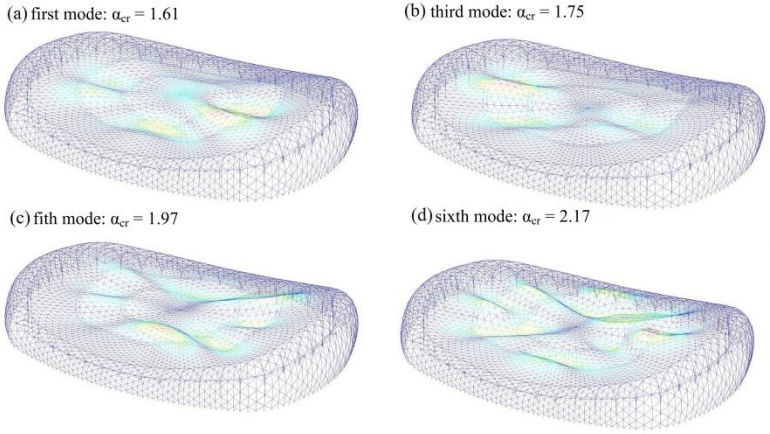

Figure 15. Typical modes of global stability loss and critical load multipliers of the structure [12]

The previous consequences are lead to the modification of the structure: the first critical load multiplier is increasable by placing a spatial truss as a stiffener beam along the two rings. This stiffener truss can block the fluctuant buckling modes. The stiffeners can be configured expediently as a triangular spatial truss. The truss itself consists of an isosceles triangle's sides, a flange which connects the isosceles triangles, and stiffener bars on the sides of the triangle truss (Fig.16.).

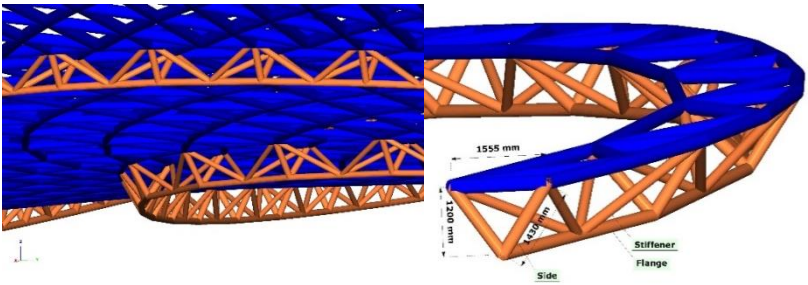

Figure 16. The performance of one triangular spatial truss [12]

The triangle's three different heights were examined: a height of 900 mm, 1200 mm and 1500 mm, in order to find an optimal α_{cr} value by iteration. It should be mentioned, that here the parametric design was an effective tool to vary the dimensions of the triangles. The variations were exported from Rhinoceros in .dxf format and directly imported to ConSteel, where the analysis was performed. The effect of the height of these triangles on α_{cr} value can be seen in Fig. 17.

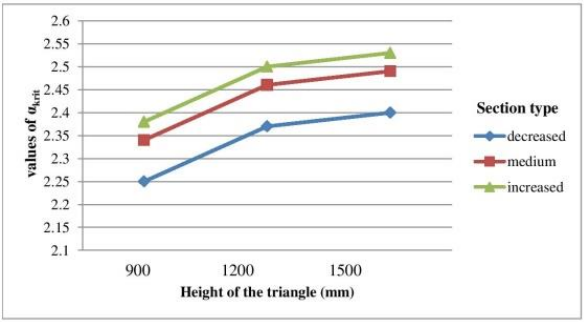

Figure 17. The effect of the height of the stiffener on critical load multiplier

The regulation EN 1993-1-1 [12] of overall imperfection method of compressed bars was used to accomplish the global stability analysis. According to the regulation the first buckling shape may be placed onto the initial perfect structural geometry (Fig. 18) with initial amplitude ($L_0/150 \cong 73$ mm) defined in favour of safety.

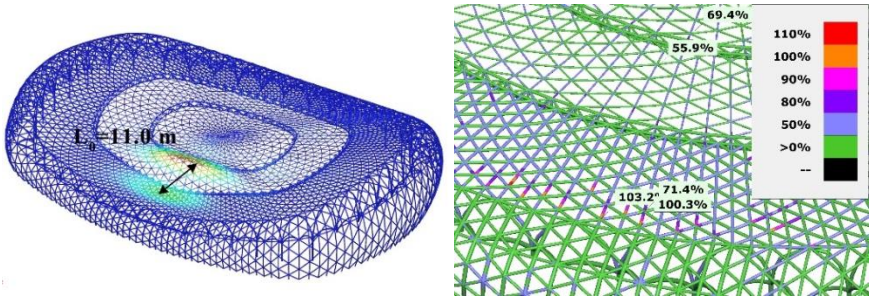

Figure 18. (i) First mode of global stability loss of the modified structure (stiffener rings) (α_{cr}=2.50), (ii) Results of the global stability analysis [12]

The dynamic behaviour of the structure is well defined by the self-oscillation's number. On Fig. 19 the first and the fourth mode of self-oscillations is shown. The lowest value of self-oscillation is 0.848 which value is high enough to preclude the excitation of the structure caused by repeating blows [19]. Irrespective of this conclusion a more precise dynamical calculation is needed by virtue of detailed analysis and designing.

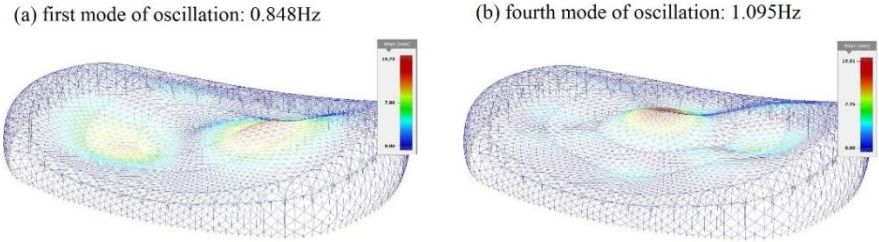

Figure 19. Modes of global self-oscillations [12]

4.5. Conceptual design of joints

As a part of the structural concept the designing of one type of joint was proposed. The selection of the joint was based on the fact which type is the commonest in the contsrtuction. Thus the chosen joint is a general intermediate joint, in which 6 beams are connected. The proportion of this kind of joint is about 80% of the construction's joints. From among these joints the most stressed had been chosen to design.

The general intermediate surface joint consist of a central joint (central element + 6 beam ends) and 6 constructional beams. Economically the most advatageous if

the beams are connected to each other with clear interaction. Thus in this case every second beam is connected to the central element with clear interaction. Thereafter the remained 3 beams only could be connected with 3-3 interactions (1 with the central element, 1-1 with the adjacent beams). The connection between the incoming beams and the central element is welded. Yet the constructional beams are connected with the obtained central joint with bolted connections. To increase the flexural rigidity and to avoid the local yieldings, cross-shaped stiffeners are welded into the headplates of the connecting constructional beams.

To model the joints a model-based on finite element method, finite strip method and shell element was used. To reduce the complexity of the model the component method was used for determining the strains of the joint elements. The 3D geometry of the joint was came from the parametric model. The input data used for modeling the joints were also parametrized. A linearly elastic and perfectly plastic material model was used to accomplish the examinations. The most important input parameters were the material behavior and the properties of the connecting elements (bolts and welds). The bolted connections were replaced by springs connected in sequence. Bolts work for tensile and shear forces, while the welded contacts transmit only compression. In case of the joints' calculation their effect for the global structural behaviour have to be examined continuously. In Fig. 20 the finite element model of the central joint is shown.

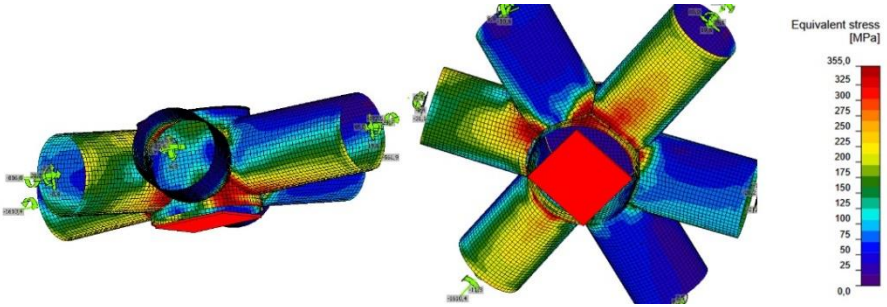

Figure 20. Equivalent stress of central joint [14]

5. Interoperability of the used architectural and structural design software

The modelling of the main form (including the structural elements and the grid) was performed in Rhinoceros 3D [7] using the Grasshopper [8] module for parametric design. For the conceptual structural design the ConSteel software [12] was used, while for design of the joints the IDEA StatiCa software was applied [14]. The model was exported in .dxf format from Rhinoceros, which is found to be an efficient method for further processing of the model. The applied software aided design method also enabled the 3D print of the structure in a scale of 1:200. The model was exported from the Rhinoceros 3D in .stl format and after checking the model adequacy, it was printed with the technology of Selective Laser Sintering (SLS). (Fig. 21)

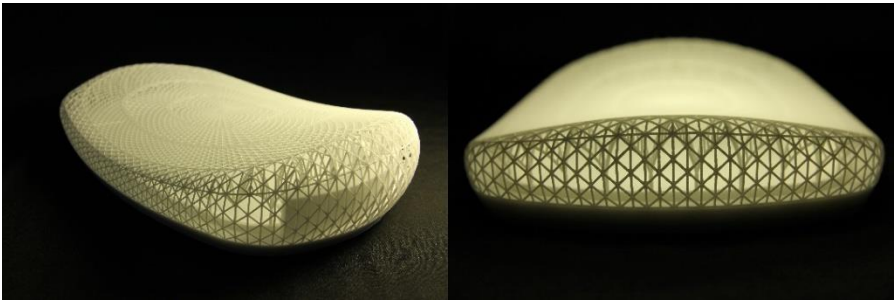

Figure 21. 3D printed model of the structure

Conclusions

With this case study the authors would like to demonstrate the advantages of the use of parametric design method in architectural and structural design projects. This method was an effective tool during the whole design process. It enabled to try different forms of the building, to vary the main dimensions of the final form in order to reach the optimal solution both functionally and architecturally. It was also used to generate and analyse different grid variations. Furthermore, the modification needed based on the structural analysis was made easier by this method. The communication between the software used was mostly quick and appropriate. As a consequence, in the course of the cooperation with structural designer the parametric design method can be a powerful tool, which made it possible to handle the effect of structural behaviour of the building on the architectural design.

References

[1] F. R. Khan, Structural aesthetics in architecture and its social and technological relevance, IABSE Congress Report Vol. 11, 1980.

[2] PriceWaterhouseCoopers, Budapest 2024: Summer Olympic and Paralympic Games – Feasibility Study, Budapest, (2015) [cited 2016-02-26] URL http://olimpia.hu/images/bp2024/PwC_Olimpiai%20Megvalosithatosagi%20tanulmany_2015_junius_vegleges.pdf, in Hungarian.

[3] Ernst Neufert, Peter Neufert: Architects' Data, 4th Edition, Wiley-Blackwell, 2012.

[4] Fédération Equestre Internationale, Dressage Rules, 25th edition, effective 1st January 2014, Including updates effective 1st January 2015, (2015) [cited 2016-03-30]. URL https://inside.fei.org/sites/default/files/DRE-Rules_2016_GA-approved_mark-up.pdf

[5] Fédération Equestre Internationale, Jumping Rules, 25th edition, 1 January 2014, Updates effective 1 January 2016, (2016) [cited 2016-03-30]. URL https://inside.fei.org/sites/default/files/JumpRules_25thEd_modifs-2016_approved_2015GA_mark-up.pdf

[6] Javier Monedero: Parametric design: a review and some experiences, Automation in Construction 9, (2000) pp. 369-377.

[7] Robert McNeel & Associates, Rhinceros 3D, [cited 2016-03-30]. URL https://www.rhino3d.com/

[8] S. Davidson, Grasshopper – Algorithmic Modeling for Rhino, [cited 2016-03-30]. URL http://www.grasshopper3d.com/

[9] G. Kiss, Integrated numerical design methods for designing of „free-form" buildings, Diploma thesis, Budapest University of Technology and Economics, Department of Structural Engineering, Budapest, 2016, in Hungarian.

[10] H. Schober, Freeform Glass Structures, (2006) [cited 2016-12-10]. URL http://www.formpig.com/pdf/formpig_freeform%20glass%20structures_schober.pdf

[11] L. Mészáros, Large-spain roof structures – steel dome structures, Magész Acélszerkezetek, 7 (2) (2010) pp. 46-51, in Hungarian.

[12] ConSteel Advanced Building Analysis Solution for Structural Engineers, ConSteel Soltutions Ltd., URL www.consteelsoftware.com

[13] MSZ EN 1993-1-1:2005/A1:2015, Eurocode 3: Design of steel structures – Part 1-1: General rules and rules for buildings

[14] IDEA StatiCa 2009-2018, [cited 2016-03-30]. URL https://www.ideastatica.com/steel/

Acta
Technica
Jaurinensis

Vol. 11, No. 2, pp. 61-83, 2018
DOI: 10.14513/actatechjaur.v11.n2.453
Available online at acta.sze.hu

Parallel Numerical Creation of 2-parametric Bifurcation Diagram of Nonlinear Oscillators

F. Hajdu

Széchenyi István University, Faculty of Mechanical Engineering, Informatics and Electrical Engineering, Department of Mechatronics and Machine Design
Egyetem tér 1., 9026 Győr, Hungary
e-mail: hajdfl@sze.hu

Abstract: This paper presents the numerical creation of 2-parametric bifurcation diagrams of nonlinear oscillators with a simple iterative algorithm, which can be easily parallelized. The parallel algorithm was tested with two simple well-known nonlinear oscillators, the Van der Pol oscillator and the Duffing-Holmes oscillator. It was examined how the resolution (number of iterations) affects the speedup and the efficiency. The test results show that a relative good speed up with a good efficiency could be achieved even using a simple desktop.

Keywords: parallel computing, bifurcation diagram, numerical analysis, nonlinear oscillator, Maple

1. Introduction

Bifurcation diagram is a very useful tool to study nonlinear dynamical systems. It shows the systems behaviour as a system parameter is varied [1]. In most cases the bifurcation diagram of a single parameter is calculated [2]-[9], but a system can have more bifurcation parameters [10]. In order to examine the effect of more bifurcation parameters at the same time a 2 parametric or 3D bifurcation diagram can be created [11]. However constructing a detailed 3D bifurcation diagram can be time consuming even in case of simple systems, as a lot of numerical calculation is necessary. These calculations can be fastened using more processor cores [12]. The aim of this research was to create 3D bifurcation diagrams within a reasonable time using simple PC-s.

The paper first presents some examples using 3D bifurcation diagrams found in the literature, then the sequential and parallel numerical creation of 3D bifurcation

diagrams are described, which is followed by some test results. The paper concludes with further development tasks.

2. Creation of bifurcation diagram with more parameters

In the literature some examples of simulations using 3D bifurcation diagrams and methods for calculating and visualizing bifurcation surfaces of more parameters can be found.

In [11], the creation of the 3D bifurcation diagram is presented with a predator-prey model. The bifurcation points are calculated with the Newton-Raphson method. Then the surface diagram is created with triangulation.

In [13], the use of different 3D bifurcation diagram is presented with population model examples, like ecosystem models and predator-prey models. A 3D bifurcation diagram with 2 state variables and a bifurcation parameter is used to determine the stability of the systems. 3D bifurcation diagrams with 3 different parameters are calculated to examine the equilibrium points and the type of bifurcations.

Reference [14] proposes an efficient algorithm to calculate and visualize three dimensional bifurcation surfaces. The algorithm was tested with a socio-economic model, a metabolic network and a food-chain model.

In [15], an analytical method based on resultant is presented to calculate bifurcation surfaces. The presented method is suitable for medium size systems and can be used to detect Hopt bifurcations and some higher codimension bifurcations too.

More parametric bifurcation diagrams have been used to study electrical systems. In [16], ferroresonance of power systems is predicted with 3D bifurcation diagrams. The 3D bifurcation diagram is produced with creating as many 2D bifurcation diagrams as the second parameter range. The 2D bifurcation diagram is created with repeating time-domain simulations followed by frequency-domain sampling of the same output to determine its periodicity. The creation of bifurcation diagram was speed up using a 50 core parallel computer [17].

In [18], the bifurcation analysis of a permanent magnet synchronous motor was achieved using 2D bifurcation curves and 3D bifurcation surfaces. The bifurcation surfaces were created from bifurcation curves calculated with different values of the third parameter.

In [19], the 3D bifurcation diagram of a simple electrical system with a nonlinear Tunnel diode is created using Maple's *implicitplot* command.

2D and 3D bifurcation diagrams can be used to examine biochemical reactions too. In [20], stable states of a protometabolic network are studied with 2D and 3D bifurcation diagrams.

The creation of 3D bifurcation diagram can be very time consuming [17]. The aim of this research was to expand a fast and efficient algorithm used to calculate 2D bifurcation diagrams in a way to create 3D bifurcation diagrams even on simple PC-s within a reasonable time.

2.1. The algorithm to create the 3D bifurcation diagram

The 2D bifurcation diagram can be created with a simple iterative algorithm based on the algorithm described in [21]. The flowchart of the algorithm can be seen in Figure 1.

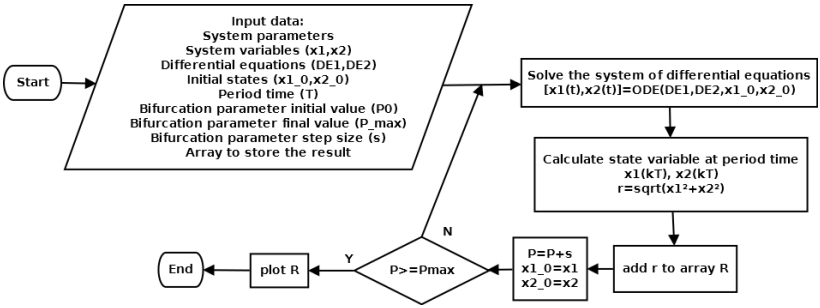

Figure 1. Algorithm to create the bifurcation diagram

The 3D bifurcation diagram can be created if the 2D bifurcation diagrams are calculated with every value of a different bifurcation parameter and the results are displayed in a 3D plot (Figure 2).

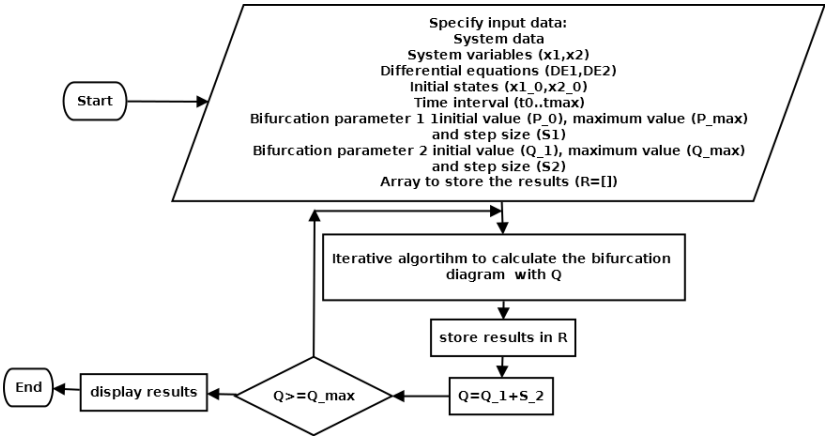

Figure 2. Algorithm to create the 3D bifurcation diagram

In this study the numerical 3D bifurcation diagram of the forced Duffing-Holmes and the forced Van der Pol oscillator is created. Maple was used as it is a powerful tool for both symbolic [22] and numerical calculations[23]. The equation of the Duffing-Holmes oscillator is:

$$\frac{d^2}{dt^2}x(t) + \delta\frac{d}{dt}x(t) + \beta x(t) + \alpha x(t)^3 = \gamma\cos(\omega t) \qquad (1)$$

In this study parameters α=1, β=-1 and ω=1 were chosen as constants and δ and γ are the bifurcation parameters. The bifurcation diagram can be seen in Figure 3.

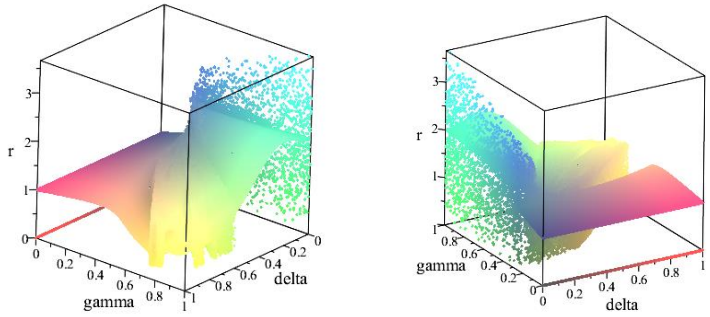

Figure 3. 3D bifurcation diagram of the Duffing-Holmes oscillator

From the diagram the bifurcation regions can be observed, which are:

- γ=0
- δ=0
- the region between γ=4/3×δ+0.2 and γ=0.6×δ+0.2

To test the accuracy of the bifurcation diagram some Poincare sections were created, which can be seen in Figure 4.

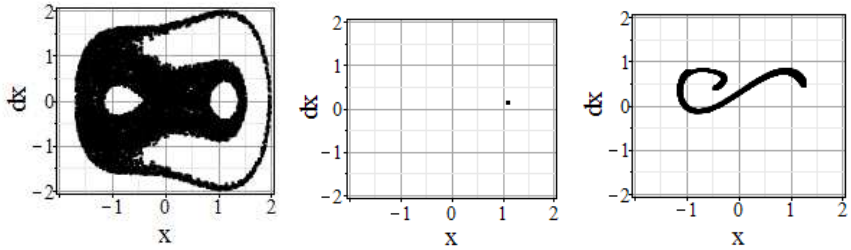

Figure 4. Poincaré sections of the Duffing-Holmes oscillator (γ=0.1 and δ=0, γ=0.2 and δ=0.8, γ=0.6 and δ=0.5)

It can be seen, that the Poincaré sections also show the chaotic behaviour at the same parameter values as the bifurcation diagrams. When γ=0.1 and δ=0 and γ=0.6 and δ=0.5 there is a chaotic oscillation and in case of γ=0.2 and δ=0.8 there is a harmonic oscillation.

The equation of the forced Van der Pol oscillator is:

$$\frac{d^2}{dt^2}x(t) = \mu(1 - x(t)^2)\frac{d}{dt}x(t) - x(t) + Acos(\omega t) \qquad (2)$$

In this study ω=2π/10 and μ and A are the bifurcation parameters. The 3D bifurcation diagram can be seen in Figure 5.

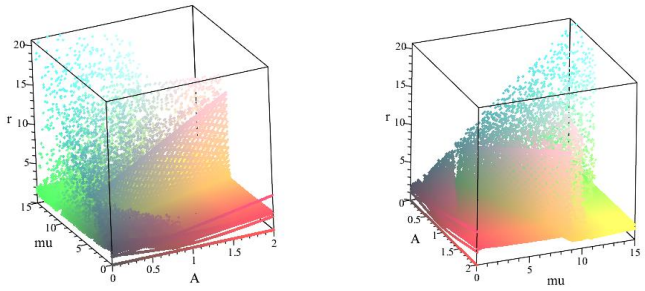

Figure 5. 3D bifurcation diagram of the Van der Pol oscillator

From the diagram the bifurcation regions can be observed, which are:

- the region μ <=10×A
- between μ =2.5×A, A=[1.2-2] and μ =10, A=[0,1.2] and μ =15, A=0

If μ =0 there is a subharmonic oscillation. Some Poincaré sections were created to test the accuracy of the bifurcation diagram with a different system too (Figure 6).

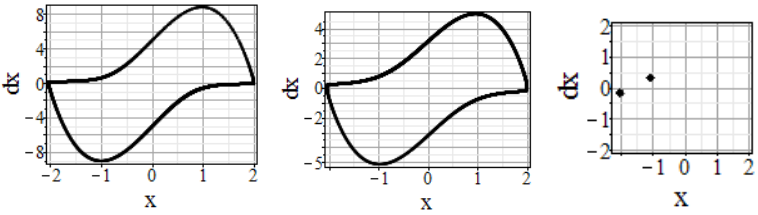

Figure 6. Poincaré sections of the Van der Pol oscillator (μ=6 and A=0.5, μ=3 and A=0.2 and μ=10 and A=1.5)

It can be seen that similarly the previous system the Poincaré sections shows the system behaviour according to the 3D bifurcation diagram: when μ =6, A=0.5 and μ =3 and A=0.2 there is a chaotic limit cycle and when μ =10 and A=1.5 there is a subharmonic oscillation.

As the same iterative algorithm is used with every values of the bifurcation parameters this task can be easily parallelized.

2.2. Parallel algorithm

The numerical creation of the 2 parametric bifurcation diagram can be parallelized with a similar algorithm presented in [24]. For parallelization Maple's Grid programming model was used. There is a master node to supervise the slave nodes and to collect the results. The slave nodes calculate the data for the bifurcation diagram for each bifurcation parameter and send the results to the master node. The flow chart of the parallel algorithm can be seen in Figure 7 and the Pseudo code of the Maple program can be seen in Figure 8.

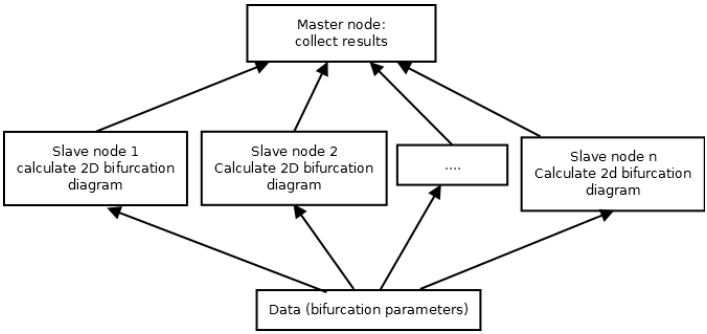

Figure 7. Flow chart of the Grid Programming model (SIMD parallel algorithm)

```
dist_lc :=proc( )

 #define variables
 #setup nodes
 this_node := MyNode( ) :
active_nodes := NumNodes( ) − 1 :

 #initialization

#set master node
if this_node = 0 then
    for iNode from 1 to active_nodes do
 #receive results from slave nodes
   end do:

 #set slave nodes
else
for i from 1 to nops(delta) do
imod := i mod active_nodes :
if imod = 0 then imod := active_nodes end if:
 if this_node = imod then

 #iterative algorith to calculate the bifurcation
 #diagram for each parameter value
end if
 #send results to master node
 end if :
 end proc:
```

Figure 8. Pseudo code of the parallel Maple program

3. Creation of bifurcation diagrams with more parameters

The tests were carried out on a PC with an Intel® Core™ i5-4460 Processor 3.2 GHz and 16 GB RAM. The processor has 4 cores

The speedup, the efficiency and the overhead of the program were calculated with the following formulas [25]-[27]:

$$S = \frac{T_s}{T_p} \tag{3}$$

$$E = \frac{S}{n} \tag{4}$$

$$O = \frac{T_p - T_u}{T_p} \tag{5}$$

where T_s is the sequential calculation time, T_p is the parallel running time, T_u is the time of the useful work (calculation time of a 2D bifurcation diagram), n is the number of cores.

To change the resolution of the bifurcation diagram the number of iteration was varied for both parameters:

$$resolution = \frac{1}{N} \tag{6}$$

where N is the number of iterations. The number of iterations for each resolution can be seen in Table 1. G is parameter of the iterative algorithm to create a single bifurcation diagram (γ and μ) and D is the parameter for the number of bifurcation diagrams in 3D (δ and A).

Table 1. Number of iterations as resolution of the bifurcation parameters (G and D) is changed

	D	**11**	**26**	**51**	**101**	**251**	**501**	**1001**
G								
11		121	286	561	1111	2761	5511	11011
26		286	676	1326	2626	6526	13026	26026
51		561	1326	2601	5151	12801	25551	51051
101		1111	2626	5151	10201	25351	50601	101101
251		2761	6526	12801	25351	63001	125751	251251
501		5511	13026	25551	50601	125751	251001	501501
1001		11011	26026	51051	101101	251251	501501	1002001

3.1. Duffing-Homes oscillator

In case of the Duffing-Holmes oscillator set [0,1] was given for both bifurcation parameters. The calculation times as the resolution of γ is varied can be seen in Figure 9.

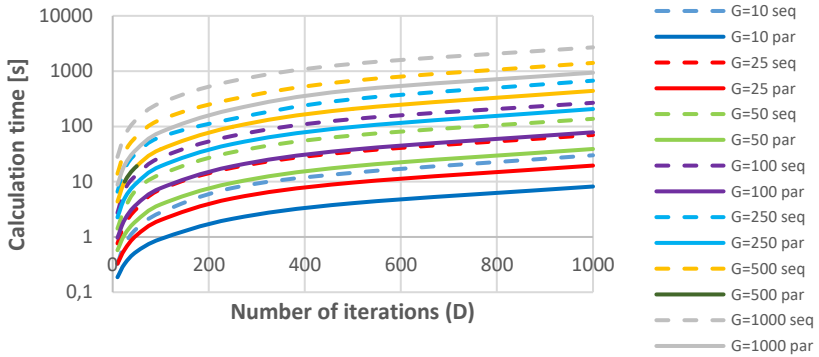

Figure 9. Calculation times versus the resolution (different resolution for G) in case of the Duffing-Holmes oscillator

It can be seen that the calculation time increases as the resolution is increased. The calculation time of the parallel algorithm is less than 1000 s at the highest resolution. The speedup and the efficiency are shown in Figure 10.

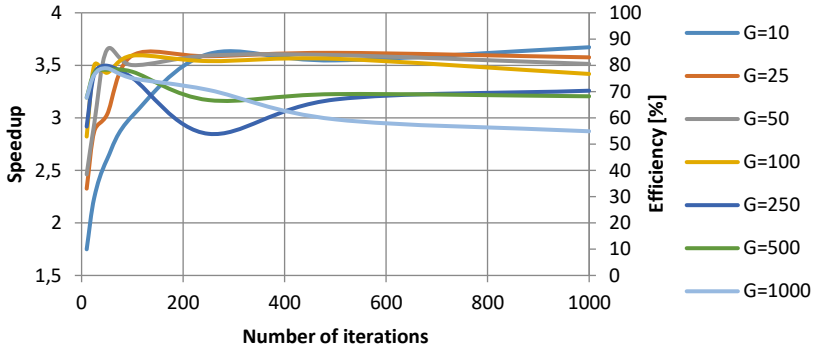

Figure 10. Speedup and efficiency versus the resolution (different resolution for G) in case of the Duffing-Holmes oscillator

From Figure 10 the following can be derived:

- When G=10 and D is small S<2 and E<50%. When G is increased both of them increases. When D=1000 S>3.6 and E>91%. It is the best result achieved.
- When G=25 and G is small S<2.5 and E<60%. When D is increased both increases fast and when D>100 an approximately constant S=3.58 and E=90% can be achieved.
- When G=50 and G is small S=2.5 and E=60%. When D is increased first there is a fast increase in G and D. The best results could be achieved, when D=50, in this case S>3.6 and E>91%. When D is increased further first there is a decrease in both. An average S=3.5 and S=89% could be achieved.
- When G=100 and D is small S=2.8 and E=70%. When D is increased there is an increase in both. The best result could be achieved, when D=100. In this case S=3.6 and E=90%. When D is further increased both of them decreases, but E>85% remains.
- When G=250 and D is small S=2.9 and E=72%. When D is increased both of them increases (till D=50), then they decrease (till D=250) and then they increase again till S=3.25 and E=81%. The best results could be achieved when D=50 and the worst results when D=250.
- When G=500 and D is increased (till D=50) S and E increase, after they decrease (till D=250) and after a small increase they remain constant (S=3.22 and E=80%).
- When G=1000 and D is increased after a short increase S decreases from 3.5 to 2.8 and E decrease from 87% to 72%. At this resolution lack of memory also occurred.

The overhead is shown is Figure 11.

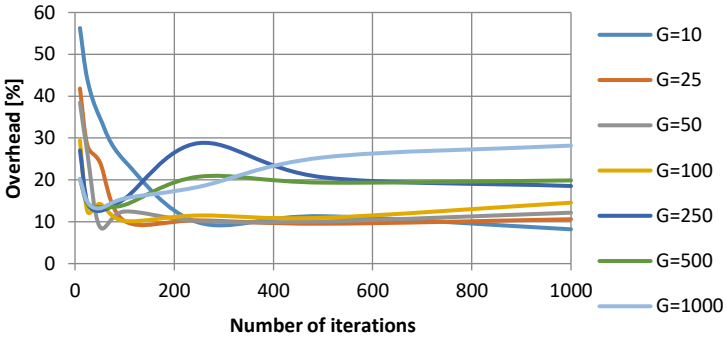

Figure 11. Overhead versus the resolution (different resolution for G) in case of the Duffing-Holmes oscillator

From Figure 11 the following can be derived:

- When the resolution is small the overhead is high (40-60%), which means the communication time between the nodes is high compared to the useful calculation time
- The overhead increases (till almost 30%) when G=1000 and the resolution is increased
- The overhead is increased till 20% when G=250 and G=500 and the resolution is increased
- All the other cases the overhead is 10%, which means only 10% of the total running time is spent on the communication

The effect of different G and D values in case of the same number of iterations to efficiency and overhead was also compared. The results can be seen in Figure 12.

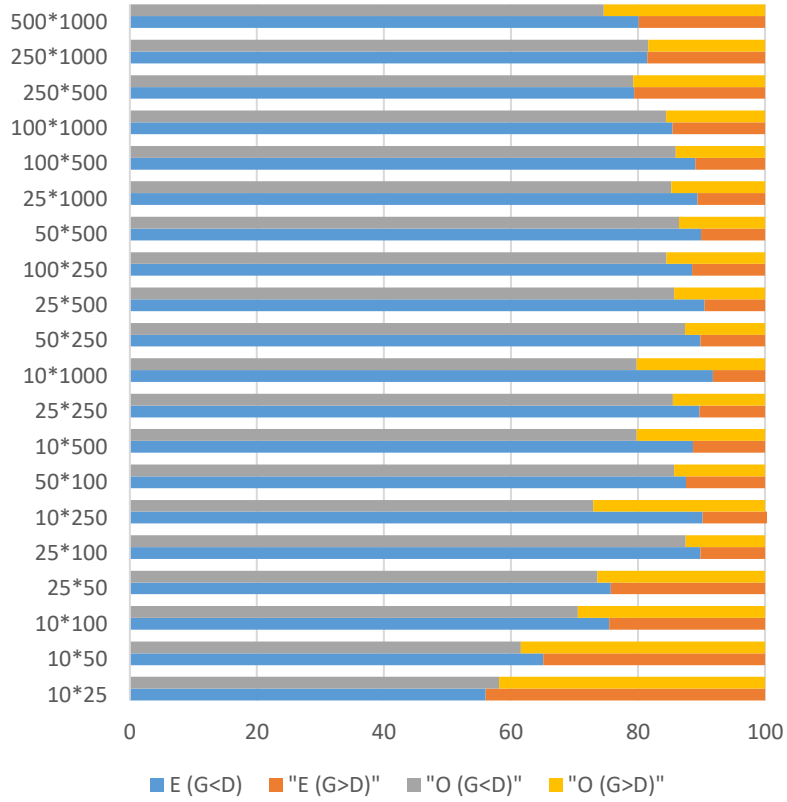

Figure 12. Comparison of efficiency and overhead with different G and D values at the same number of iterations in case of the Duffing-Holmes oscillator

It can be seen that except the smallest resolution the speedup and efficiency were better, when G<D. It means that it is more effective to calculate a lot of low resolution 2D bifurcation diagram in parallel, that to calculate a low amount of high resolution 2D bifurcation diagrams.

The average difference is 4%. The smallest difference is at resolution 500×250 and 1000×250, it is <20% is both cases. The difference was small (<3%) in resolution 10×25, 25×50, 25×100, 50×250 and 100×1000. The maximum difference is 17.27% (means 0.69 less speedup), which is at resolution 10×250.

The overhead is also much higher at this resolution, when G>D. The difference is also high at resolution 10×500 (8.84%) and 10×1000 (12%). It also shows that it is not efficient to calculate small number of detailed 2D bifurcation diagrams in parallel, as communication can be time consuming.

Figure 13. shows the average speedup, efficiency and overhead versus the average number of iterations.

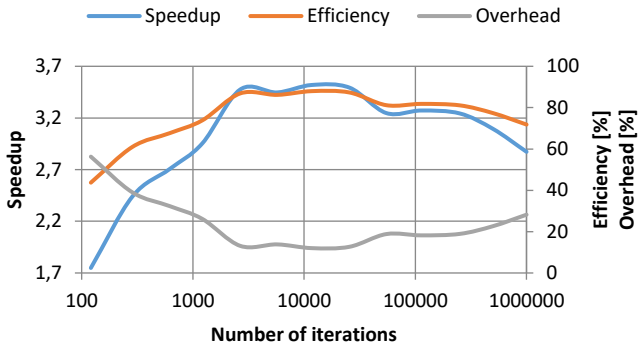

Figure 13. Average speedup, efficiency and overhead versus the average number of iterations in case of the Duffing-Holmes oscillator

It can be seen that S and E increases till the number of iterations is 12000, after it decreases. The speedup is still >3 and the efficiency is 77% with 500000 iterations. The average overhead first is above 40% and when the resolution is increased (around 3000 iterations) it desreases under 20%.

3.2. Van der Pol oscillator

For this test A=[0,2] and μ =[0,15] sets were given. The calculation times as the resolution of μ is varied can be seen in Figure 14.

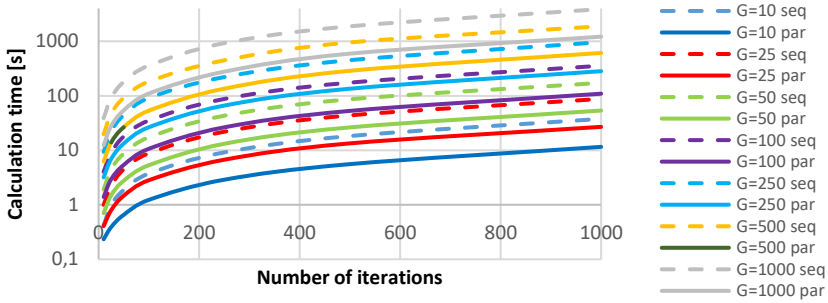

Figure 14. Calculation times versus the resolution (different resolution for G) in case of the Van der Pol oscillator

It can be seen that the calculation time increases as the resolution is increased. The calculation time of the parallel algorithm is less than 1500 s at the highest resolution. The speedup and the efficiency are shown in Figure 15.

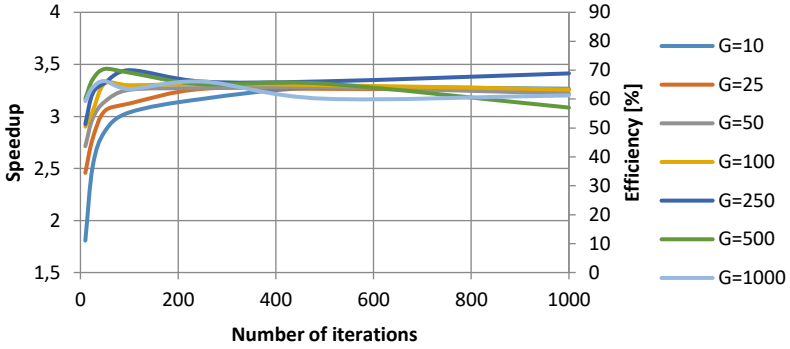

Figure 15. Speedup and efficiency versus the resolution (different resolution for G) in case of the Van der Pol oscillator

From Figure 15 the following can be derived:

- When G=10 and D is small S<2 and E<50%. When G is increased both of them increases till S=3.2 and E=81%.

- When G=25 and G is small S=2.5 and E=61%. When D is increased both increases fast and when D>250 an approximately constant S=3.2 and E=81% can be achieved.
- When G=50 and G is small S=2.7 and E=67%. When D is increased till 500 both of them increases till S=3.28 and E=82%. When D is further increased there is a small decrease in E and S.
- When G=100 and D is small S=2.9 and E=72%. When D is increased till 500 there is an increase in both till S=3.3 and E=82%. When D is further increased there is a small decrease in both of them.
- When G=250 and D is small S=2.9 and E=73%. When D is increased both of them increases till D=100 (S=3.4 and E=86%). When D is further increased first there is a small decrease (till D=500) and then a small increase in both.
- When G=500 and D is increased (till D=50) S and E increase. This is the best result achieved: S=3.45 and E=86%. After that they decrease till S=3.1 and E=77%.
- When G=1000 and D is increased after a short increase S decreases from 3.3 to 3.2 and E decreases from 83% to 80%.

The overhead is shown is Figure 16.

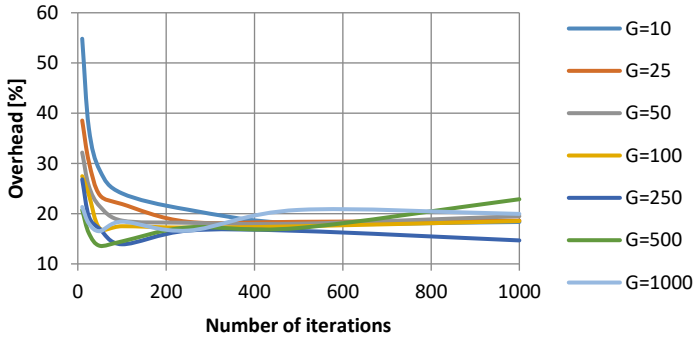

Figure 16. Overhead versus the resolution (different resolution for G) in case of the Van der Pol oscillator

From Figure 16 the following can be derived:

- When the resolution is small the overhead is high (40-55%), which means the communication time between the nodes is high compared to the useful calculation time
- The overhead increases (till almost 25%) when G=500 as the resolution is increased
- The overhead is increased above 20% when G=1000 and the resolution is increased
- All the other cases the overhead is <20%, which means less than 20% of the total running time is spent on the communication

The effect of different G and D values in case of the same number of iterations to efficiency and overhead was also compared. The results can be seen in Figure 17.

It can be seen that most cases the speedup and efficiency were better (and the overhead lower), when G>D, only at some higher resolution cases were the efficiency better in case of G<D. It means that similarly to the Duffing-Holmes oscillator it is more efficient to create a lot of low resolution 2D diagrams, than to create a smaller number of higher resolution 2D diagrams in parallel.

The average difference is 2.3%. The smallest difference is at resolution 100×1000 and it is <0.15%. The difference is less than 4% in almost all cases except resolution 250×10 (6.04%) and resolution 500×50 (4.4%). The difference in overhead is also higher at these resolutions. The difference in efficiency and overhead was much less than the difference with the Duffing-Holmes oscillator, which means that the tasks could be divided between the nodes more effectively.

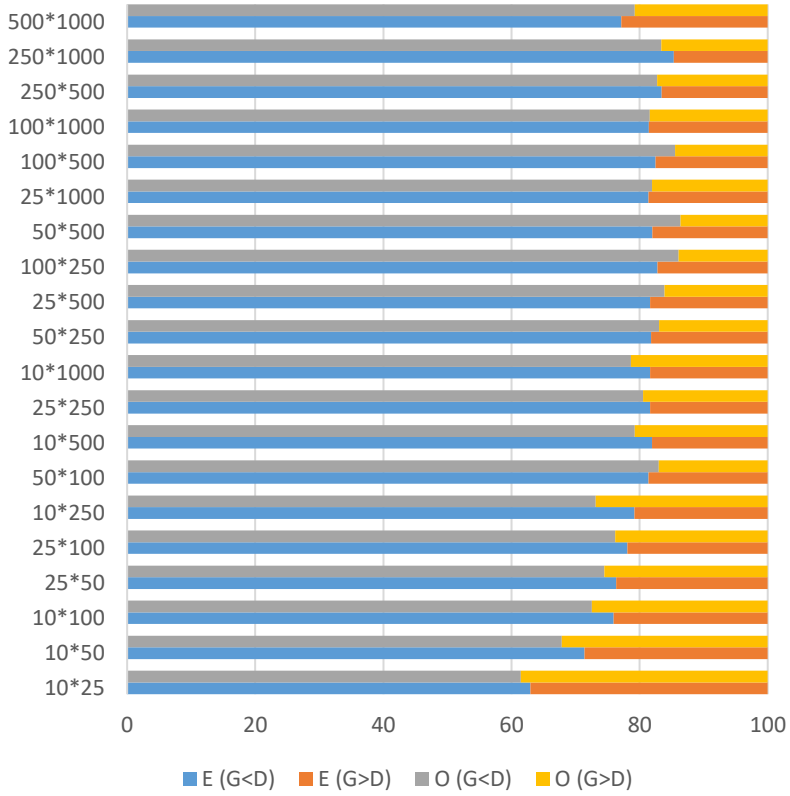

Figure 17. Comparison of efficiency and overhead with different G and D values at the same number of iterations in case of Van der Pol oscillator

Figure 18 shows the average speedup, efficiency and overhead versus the number of iterations.

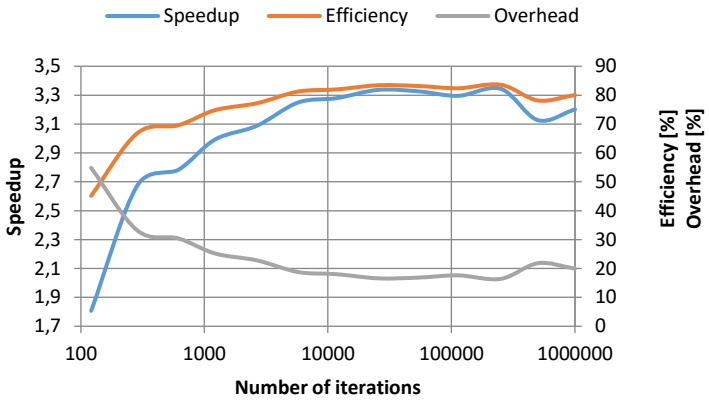

Figure 18. Average speedup, efficiency and overhead versus the number of iterations in case of the Van der Pol oscillator

It can be seen that S and E increases till the number of iterations is 25000, after it is nearly constant (S=3.3 and E=83%) till number of iterations is 250000, ather that it decreases. The speedup is still >3.1 and the efficiency is 78%. The average overhead is first >40% and when the resolution is increased (around 6000 iterations) it desreases under 20%.

4. Conclusions and further development

The parallel numerical creation of a 3D bifurcation diagram of two simple nonlinear oscillators was carried out with a simple and fast iterative algorithm. An average 3-fold speedup could be achieved with average 76% efficiency in both cases. The best results could be achieved with the Duffing-Holmes oscillator, when the number of iteration was 12000 (3.5-fold speedup and 87% efficiency). A better speedup and efficiency could be achieved with the Duffing-Holmes oscillator when the number of iteration was between 2000 and 50000 as it can be seen in Figure 19. At all other resolutions the results were better with the Van der Pol oscillator. The average overhead was high till 3000 iterations (30-40%), then it was <20% till 100000 iteraritons in both cases. When the resolution is further increased the average overhead increases till 20-30% (Figure 19).

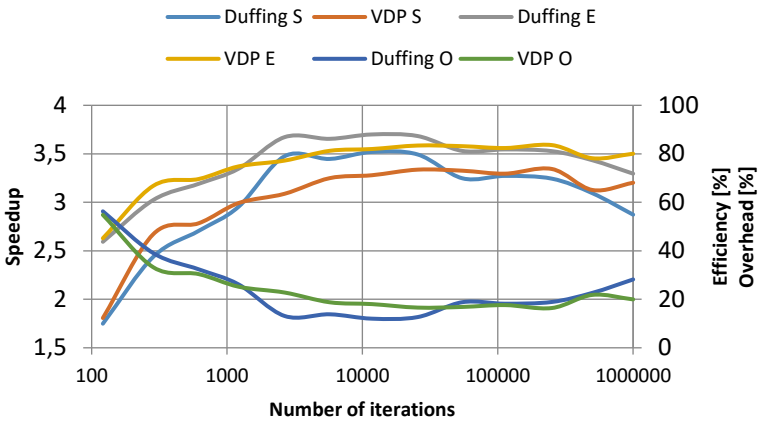

Figure 19. The average speedup, efficiency and overhead versus the number of iterations

With the presented algorithm a high resolution 3D bifurcation diagram can be created of simple systems very effectively with simple PC-s with low number of cores.

Next task is the better visualization of the results, which means using surface plot instead of point plot. Some initial experiments have already been carried out creating surface plots using Maple, but for visualization there was not enough memory.

Other task in the future is utilizing supercomputers to create even more detailed 3D bifurcation diagram of more complex systems and to create other high-calculation time diagrams, like frequency spectrum maps in parallel

Acknowledgement

EMBERI ERŐFORRÁSOK MINISZTÉRIUMA

The publishing of this paper was supported by the ÚNKP-17-3 New National Excellence Program of the Ministry of Human Capacities.

References

[1] Y.A. Kuznetsov: Elements of applied bifurcation theory, Springer, 1998.

[2] G. Stépán, R. Szalai, S. J. Hogan: The Chaotic Oscillations of Highspeed Milling, In: G. Rega, F. Vestroni (eds) IUTAM Symposium on Chaotic Dynamics and Control of Systems and Processes in Mechanics. Solid Mechanics and its Applications, vol 122. Springer, Dordrecht, 2005, pp. 147-158, doi: 10.1007/1-4020-3268-4_14

[3] T. L. Schmitz, A. Honeycutt: The Extended Milling Bifurcation Diagram, Procedia Manufacturing, Vol. 1, pp. 466-474, 2015, doi: 10.1016/j.promfg.2015.09.005.

[4] H. Marzbani,M. Fard, R. Jazar: Chaotic Behavior of Hydraulic Engine Mount, Procedia Computer Science, Vol. 96, 2016, pp. 1597-1608, doi: 10.1016/j.procs.2016.08.207

[5] J. Fakhraei, H.M. Khanlo, M. Ghayour: Chaotic behaviors of a ground vehicle oscillating system with passengers, Scientia Iranica. Vol. 24. No. 3, 2015, pp. 1051-1068. doi: 10.24200/sci.2017.4088.

[6] T. Salau: Bifurcation Diagrams of Nonlinear RLC Electrical Circuits, International Journal of Science and Technology, Vol. 1 No. 3, 2011, pp. 126-139,

[7] I.Flegar, D. Pelin, D. Zacek: Bifurcation diagrams of the buck converter, 9th International Conference on Electronics, Circuits and Systems, Dubrovnik, Croatia, Paper 7562243, 2002, doi: 10.1109/ICECS.2002.1046412

[8] L. Houfek, M. Houfek, J. Krejsa, C. Kratochvíl, J. Kolácny, P. Nykodym: Bifurcation and Chaos in Electromechanical Drive Sysstems with Small MPTPRS, Engineering MECHANICS, Vol. 15 No. 5, 2008, pp. 329-336

[9] C. Kratochvíl, M. Houfek , J. Koláčný, R. Kříž, L. Houfek , J. Krejsa: Chaos in drive systems, Applied and Computational Mechanics Vol. 1, pp. 121-126,

[10] P. Simon: Differential Equations and Dynamical Systems (in Hungarian). Eötvös Loránd University, lecture notes, Budapest, Hungary, 2013 [cited 2018.01.14.],

http://www.tankonyvtar.hu/hu/tartalom/tamop412A/2011_0025_mat_11/index.html

[11] D. Stiefs, E. Venturino, U. Feudel: Computing 3D Bifurcation Diagrams, AIP Conference Proceedings Vol. 1048 No. 1, 2008, doi: 10.1063/1.2991095

[12] L. Környei: Computation Techniques in a High Performance Parallel Simulation of Gas Dynamics in a Combustion Chamber. Acta Technica Jaurinensis, Vol. 4. No. 4., 2011, pp. 443-452

[13] B. W. Kooi: Numerical Bifurcation Analysis of Dynamical Systems, Faculty of Earth and Life Sciences, Department of Theoretical Biology, Vrije University, The Netherlands, lecture notes, 2009, [cited 2018.01.31], http://www.bio.vu.nl/thb/course/mri/mri_syllabus.pdf

[14] D. Stiefs, T. Gross, R. Steuer, U. Feudel: Computation and Visualization of Bifurcation Surfaces, International Journal of Bifurcation and Chaos, Vol 18. No 8, 2008, pp. 2191-2206, doi: 10.1142/S0218127408021658

[15] T. Gross, U. Feudel: Analytical Search for Bifurcation Surfaces in Parameter Space, Physica D: Nonlinear Phenomena, Vol. 195, No. 3-4, 2004, pp. 292-302, doi: 10.1016/j.physd.2004.03.019

[16] J. A. Corea-Araujo, F. González-Molina, J. A. Martínez: Tools for Characterization and Assessment of Ferroresonance Using 3-D Bifurcation Diagrams, IEEE Transactions on Power Delivery, Vol. 29 No. 6, 2014, pp. 2543-2551, doi: 10.1109/TPWRD.2014.2320599

[17] G. Guerra, J. A. Corea-Araujo, J. A. Martinez-Velasco, F. González-Molina: Generation of Bifurcation Diagrams for Ferroresonance Characterization Using Parallel Computing, The European EMTP-ATP Users Group (EEUG) Conference, Grenoble, France, 2015

[18] W. Souhail, H. Khamari, M. F. Mimouni: From 2D to 3D Bifurcation Structures in Field Oriented Control of a PMSM, Journal of Electrical & Electronic Systems, Vol 5. No 3., Paper 1000196, 2016, doi: 10.4172/2332-0796.1000196

[19] F. Hajdu F., Gy. Molnárka: Numerical examination of a system model with a nonlinear component, TEAM 2016: Proceedings of the 8th International

Scientific and Expert Conference, Trnava, Slovakia, 2016.10.19-2016.10.21., 2016. pp. 12-16.

[20] G. Piedrafita, K. Ruiz-Mirazo, P.-A. Monnard, A. Cornish-Bowden, F. Montero: Viability Conditions for a Compartmentalized Protometabolic System: A Semi-Empirical Approach, PLoS ONE, Vol. 7 No. 6, Paper e39480, 2012, doi: 10.1371/journal.pone.0039480

[21] S. Lynch: Dynamical systems with applications using maple, Birkhäuser Boston, 2010.

[22] Maróti Gy. Investigating parameterized model of n-gonal wheel's motion, *Pollack Periodica*, Vol. 6, No. 2, 2011, pp. 25–36. doi: 10.1556/Pollack.6.2011.2.3.

[23] Perjési-Hámori I. Two dimensional mathematical model of heat-transmission using MAPLE, *IFAC-PapersOnLine*, Vol. 48, No. 1, 2015 pp. 689–690. doi: 10.1016/j.ifacol.2015.05.207

[24] F. Hajdu, Gy. Molnárka: Parallelization of Numerical Examination of Nonlinear Systems using Maple, in P. Iványi, B.H.V. Topping, G. Várady, (Eds) Proceedings of the Fifth International Conference on Parallel, Distributed, Grid and Cloud Computing for Engineering, Civil-Comp Press, Stirlingshire, UK, Paper 30, 2017. doi:10.4203/ccp.111.30

[25] L. Környei, G. Kallós, D. Fülep: Parallel Computations on the Blade Server at Széchenyi István University, Acta Technica Jaurinensis, Vol 3. No. 1, 2010, pp. 111-126

[26] D.E. Womble, "The challenge of massively parallel computing, Parallel Computing" in E. H. D'Hollander,G. R. Joubert, F.J. Peters, H.J. Sips (Eds) Parallel Computing: Fundamentals and Applications: Proceeding of the International Conference ParCo99, Imperial College Press, 2000, pp. 32-43, doi: 10.1142/9781848160170_0003

[27] D. Petcu: Performance Metrics for Parallel Programs, lecture notes, West University of Timisoara, Romania, 2010, [cited 2018.04.30], http://web.info.uvt.ro/~petcu/calcul/PC-2.pdf

Acta
Technica
Jaurinensis

Vol. 11, No. 2, pp. 84-103, 2018
DOI: 10.14513/actatechjaur.v11.n2.456
Available online at acta.sze.hu

Uniaxial Tension of a Filament-wound Composite Tube at Low Temperature

Gy. Szabó [1], K. Váradi [1]

[1]Budapest University of Technology and Economics, Department of Machine and Product Design
Bertalan Lajos Street 3, 1111 Budapest, Hungary
e-mail: szabo.gyula@gt3.bme.hu

Abstract: The aim of this article is to model mechanical behavior of a filament-wound, rubber-based composite tube subjected to uniaxial tension at low temperature by test experiments and FE simulations. Uniaxial tensile tests at sub-zero temperature (-40 °C) have been carried out on standard test specimens and on hose pieces. furthermore, a uniaxial tensile test has been performed on a hose piece at room temperature as a reference experiment. Reinforcement layers of the composite tube are modeled as transversely isotropic, whereas elastomer liners are described by 2 parameter Mooney-Rivlin hyperelastic material model. Temperature-dependence of elastic constants of composite layers is attributed to the temperature-dependence of rubber, so uniaxial tensile tests on standard test specimens needed to be carried out for determining material properties of rubber at sub-zero temperature (-40°C).
Force-displacement results of FE models and experiments of standard test specimen and hose piece show good agreement. Likewise, force-displacement curves of reference experiment (carried out at room temperature) and its related FE simulation are in good agreement with each other. Slope of force-displacement curves of hose piece at -40 °C is nearly 3.4 times the slope of force-displacement curves of hose piece at room temperature.

Keywords: filament-wound composite tube, rubber-based tube, FE model, uniaxial tension, tensile test, material properties at -40 °C, sub-zero temperature

1. Introduction

Filament-wound composite tubes are widely used in a number of industrial fields in a wide temperature range, in oil industry, in transportation and aeronautics due to their favorable strength-to-weight and stiffness-to-weight ratio and corrosion resistance. [1]. Filament-winding is the most extensively used manufacturing process because of high volume fraction, low void content and good automation capability [2]. The most commonly encountered operational loads are: internal pressure, uniaxial and biaxial loading, and bending. For balancing internal forces, winding angles of $\pm\Theta$ are typically adopted. Winding angle of a layer is usually set to $\pm 55°$, which is the optimal value regarding biaxial loading (combined internal pressure and axial loading) [3,4]. Utilization of rubber as the matrix component gives high flexibility and toughness. One efficient method of acquiring material properties of a composite is performing uniaxial tensile test on a standard test specimen cut from the hose or on a hose piece itself.

Mechanical characterization of composite tubes is most frequently carried out by finite element models [5]. Utilization of formulae of rules of mixture is the most frequent practice for determining elastic constants of a composite. Elastic constants are derived from material properties of the reinforcing yarn and the matrix. In most FE models, plies are modeled as laminates whose elastic constants are generally obtained with the use of the rules of mixtures [6].

In cold environment, modulus of elasticity of matrix increases significantly, while modulus of elasticity of yarns is regarded as constant. Yarn waviness persists, and the resulting load distribution across all yarns becomes less uniform. Therefore, at low temperatures some yarns will share more load than others and fail earlier, resulting in progressive failures of other yarns, thus strength of the composite diminishes [7, 8]. Because the growth in the modulus of elasticity of matrix, during uniaxial tension of the composite tube, the role of the matrix becomes more prominent [9].

Micromechanical behavior of composites also changes with temperature. While at room temperature, matrix cracking has a crucial role in crack initiation; at low temperature, yarn-matrix debonding is much more characteristic because yarn-matrix interface becomes weaker [10].

In this paper, mechanical behavior of a filament-wound composite tube utilized for the passage of air in rail brake systems is investigated. Determination of mechanical properties at low temperature (-40°C) is presented in detail as well as the comparison of mechanical behavior of the composite tube at low temperature (-40 °C) and room temperature.

2. Structure and material model of composite tube

2.1. Structure of composite tube

Inner diameter of the composite tube is 28 mm, its outer diameter is 44 mm, the rubber liners are 2.4 mm thick. There are 4 reinforcement plies consisting of natural yarns and rubber matrix. The material coordinate systems of the plies are cylindrical, the layup is [+55/-55/+55/-55] [°] with respect to the axis of the tube (Figure 1).

Reinforcement plies are surrounded by rubber liners, made of EPDM-EVA copolymer, whose leading role is sealing and protecting reinforcement plies from mechanical impacts.

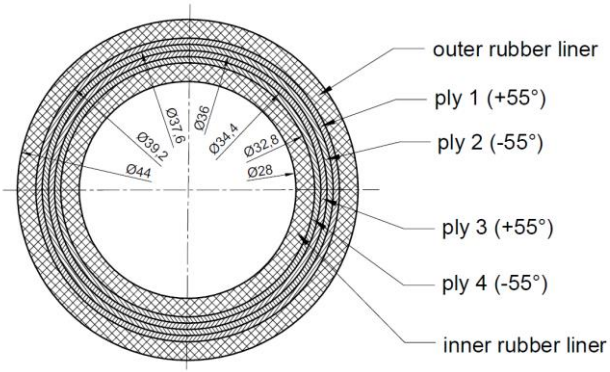

Figure 1. Cross-section of the tube [13]

2.2. Material model of composite tube

Material behavior of composites can be described by an anisotropic model in the most general case. Since in this case, the number of independent elastic constants is relatively high (21), obtainment of elastic constants tends to be challenging. Thus generally, the highest order of symmetry is taken into account. Filament-wound composite tubes are most commonly regarded as transversely isotropic because of being uniaxially reinforced, having 3 mutually perpendicular planes of symmetry, the one perpendicular to the yarns is a plane of isotropy (E_2=E_3, G_{12}=G_{13}, υ_{12}= υ_{13}). Therefore, the number of independent elastic constants can be reduced to 5 (E_1, E_2, G_{12}, G_{23}, υ_{12}) [11].

Poisson's ratio of the yarn is assumed to be ν_f =0,2, the Poisson's ratio of the rubber is supposed to be ν_m=0.5 because the rubber is regarded as incompressible. Elastic constants can be determined based on material parameters modulus of elasticity of fiber (E_f), modulus of elasticity of matrix (E_m) and fiber volume fraction (V_f).

Modulus of elasticity of fiber at -40°C equals modulus of elasticity of fiber at room temperature (E_f=2961 MPa), because its temperature-dependence is negligible. Fiber volume fraction is V_f=45% [13].

Material of the matrix is the same rubber as the liners are made of, because in the course of manufacturing, rubber of rubber liners is vulcanized around yarns. In case of rubber, temperature-dependence is significant [7], therefore for determining elastic constants at -40°C, it is inevitable to obtain modulus of elasticity of rubber at -40 °C. For this reason, standard test specimen has been cut from the outer rubber liner and has been subjected to uniaxial tension. Modulus of elasticity of rubber at -40 °C has been determined based on these tensile test results. The calculation method of elastic constants of reinforcement plies is as follows [13]:

Matrix volume fraction is:

$$V_m = 1 - V_f = 1 - 0.45 = 0.55 \tag{1}$$

Shear modulus of fiber is:

$$G_f = \frac{E_f}{2 \cdot (1+\nu_f)} \tag{2}$$

Modulus of elasticity in direction 1 is:

$$E_1 = E_f \cdot V_f + E_m \cdot V_m \tag{3}$$

Applying the formulae presented in [11] and [12], the modulus of elasticity in directions 2 and 3 and shear moduli are:

$$E_2 = E_3 = \frac{E_m}{1-\sqrt{V_f}\cdot(1-E_m/E_f)} \tag{4}$$

$$G_{12} = G_{13} = G_{23} = \frac{G_m}{1-\sqrt{V_f}\cdot(1-G_m/G_f)} \tag{5}$$

Since G_{f12}=G_{f23}, we can state that G_{12}=G_{23}.

Poisson's ratios of one ply are [6]:

$$\upsilon_{12} = \upsilon_{13} = V_f \cdot \upsilon_f + V_m \cdot \upsilon_m \tag{6}$$

Contraction in plane 23 is mainly determined by the mechanical behavior of rubber, so

$$\upsilon_{23} = \frac{E_{22}}{2 \cdot G_{23}} - 1 \tag{7}$$

2.3. Uniaxial tensile test of rubber test specimen, material properties of rubber

The test specimen has been cut in thickness direction in accordance with standard ASTM D638, thus the thickness of the test specimen is 2.4 mm, equal to the thickness of the outer rubber liner. Lateral section of the rubber test specimen, along with its dimensions, can be viewed in Figure 2. The traction of the test specimen has been conducted to a displacement of 16.5 mm, at which the specimen has ruptured. Force-displacement results have been measured during the tensile test.

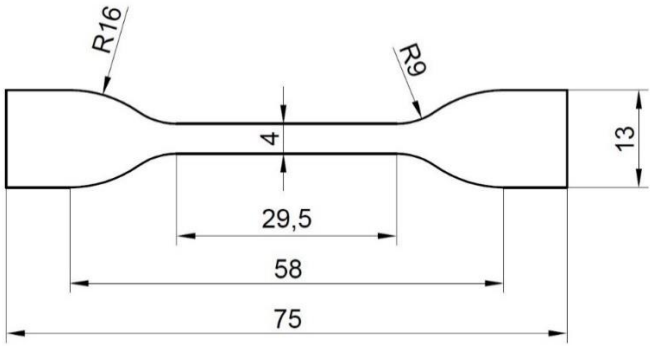

Figure 2. Lateral section of rubber test specimen [13]

Engineering stresses can be calculated based on initial cross-section A_0 = 11.2 mm^2 and measured traction force F.

$$\sigma = \frac{F}{A_0} \tag{8}$$

By using distance between grips l_0=55 mm and change in length Δl, engineering strains can be calculated:

$$\varepsilon = \frac{\Delta l}{l_0} \tag{9}$$

Resulting engineering stresses can be viewed as a function of resulting engineering strains in Figure 3.

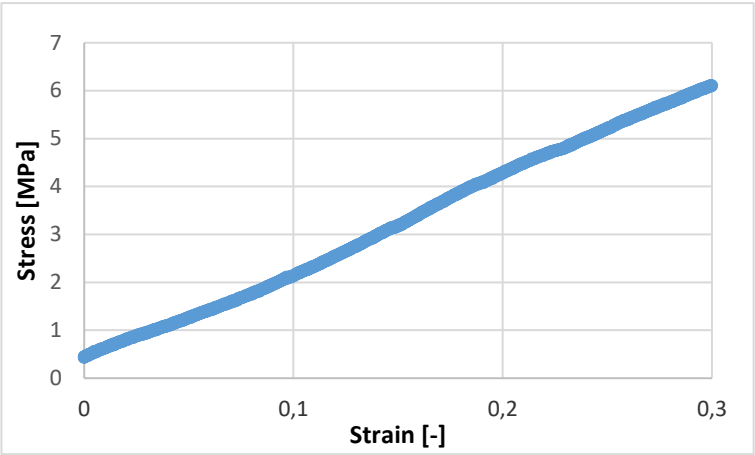

Figure 3. Stress-strain curve of rubber test specimen at -40 ˚C

Modulus of elasticity of matrix can be determined as follows:

$$E_m = \frac{\sigma_2 - \sigma_1}{\varepsilon_2 - \varepsilon_1} = \frac{6{,}11\ \text{MPa} - 0{,}44\ \text{MPa}}{0{,}3 - 0} = 18.91\ \text{MPa} \qquad (10)$$

According to data provided by the manufacturer, Shore hardness of the rubber at -40 °C is H=95 ShA.

Shear modulus of rubber can be estimated based on Shore hardness of the rubber [14]:

$$G_{r,est} = 0.086 \cdot 1.045^H = 5.63\ \text{MPa} \qquad (11)$$

Modulus of elasticity of rubber can be estimated with use of the estimated shear modulus of rubber:

$$E_{r,est} = 2 \cdot (1 + \upsilon_r) \cdot G_{r,est} = 16.89\ \text{MPa} \qquad (12)$$

The modulus of elasticity of rubber estimated with the use of Eq (12) [14] is approximately equal to that determined based on tensile test experiment. Material properties of reinforcement plies at -40°C with the use of modulus of elasticity of matrix and Eq (3) -(7) are as follows:

E_1=1345 MPa, E_2=E_3=57 MPa, υ_{12}= υ_{13}=0.364, υ_{23}=0.496; G_{12}= G_{13}= G_{23}=19 MPa.

Rubber liners are described by a 2 parameter Mooney-Rivlin model (Figure 4), whose parameters have been determined by using the curve fitting feature of Ansys Academic Research [15] on the stress-strain results of rubber test specimen.

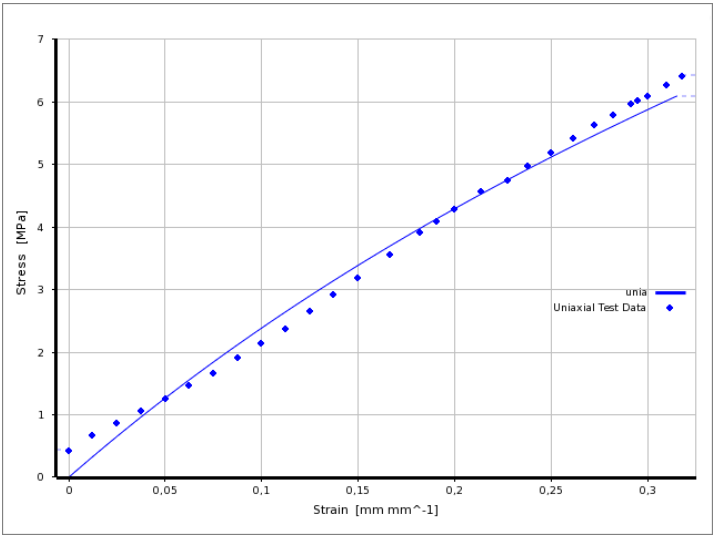

Figure 4. 2 parameter Mooney-Rivlin model fitted to stress-strain results at -40˚C

Mooney-Rivlin parameters of rubber liners are C_{10}= 2.96 MPa, C_{01}= 1.53 MPa, D=0 [1/MPa].

3. Uniaxial tension of standard test specimen at -40 °C

3.1. Tensile test experiment of standard test specimen at -40 °C

Standard test specimens have been cut from the tube in thickness direction containing both the reinforcement plies and the rubber liners, thus their thickness is 8 mm. Their lateral section is the same as depicted in Figure 2. The tensile test experiment has been performed at -40 °C in a climate chamber as depicted in Figure 5. The experiment has begun with a pre-load of 5 N. The test has been executed on a Zwick Z250 tensile testing machine with a tensile speed of 5 mm/min to complete rupture at a displacement of 11.7 mm.

Figure 5. Standard test specimen at -40 °C, placed in climate chamber

3.2. FE simulation of uniaxial tension of standard test specimen at -40 °C

Geometry of the standard test specimen is the same as that of the test experiment, its lateral section is shown in Figure 2, its thickness is 8 mm. Rigid tensile jaws have been utilized for gripping the test specimen and for executing traction.
The FE mesh comprises second order hexahedral elements to ensure the necessary precision.

3.2.1. Connections

Outer and inner rubber liners are in bonded contact with reinforcement plies. The connections of outer rubber liners and the rigid tensile jaws are frictional with a coefficient of friction of μ=0.8 with formulation 'Augmented Lagrange' [13, 16].

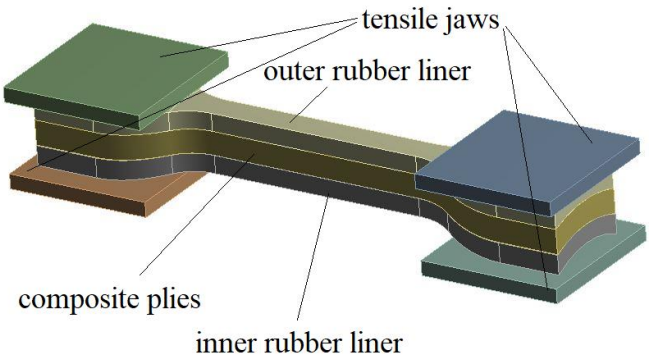

Figure 6. FE model of uniaxial tension of test specimen

3.2.2. Loads, boundary conditions

FE simulation is made up of 3 time steps. In the first and the second one, standard test specimen is being fixed between the tensile jaws. In the third time step, tension is being applied to the specimen.

In the first time step, the upper tensile jaw at the right end sinks -1.8 mm in Y direction, whereas the lower tensile jaw is still fixed (Figure 6).
In the second time step, left end of the specimen is being installed. The upper left tensile jaw descends -1.8 mm in Y direction, while the lower right tensile jaw maintains its position.

In the third time step, tensile jaws located at the right end are being displaced 11.6 mm in positive X direction.

3.3. Comparison of experimental and FE simulation results

Force-displacement results of experiment (conducted at -40 ˚C) and FE simulation of standard test specimen are shown in Figure 7.

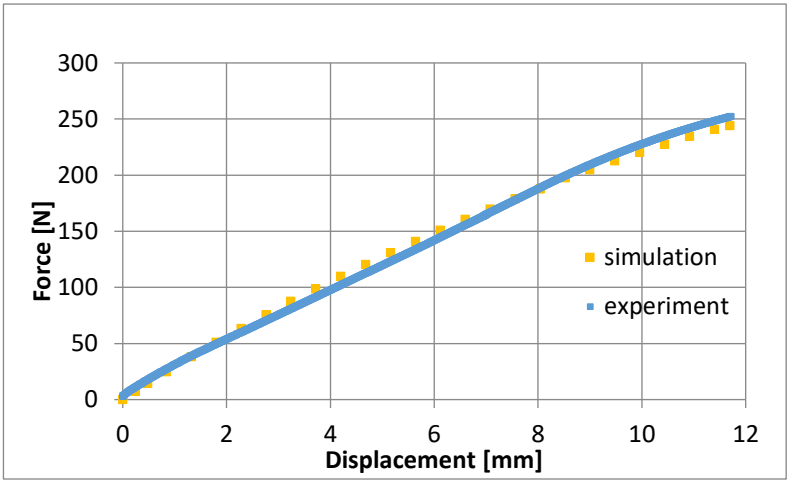

Figure 7. Force displacement curves of standard test specimen, -40 ˚C

Force displacement curves of standard test specimen are in acceptable agreement in the entire displacement range investigated.

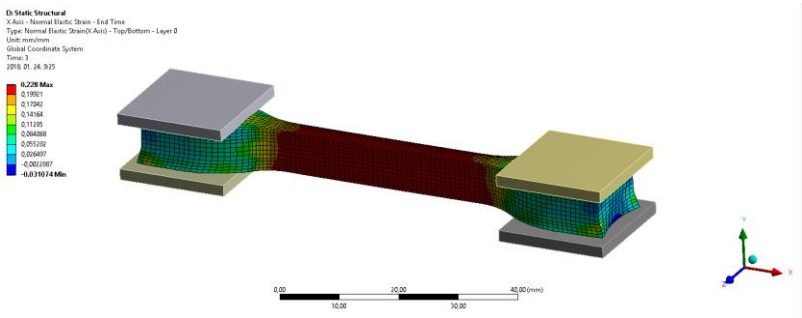

Figure 8. Strain in global X direction at the end of uniaxial tension

At the end of third time step, strain in global X direction is significant, nearly ε_x=0.23. (Figure 9)

Strain and stress results are hereinafter shown for ply 1 (outermost reinforcement ply) at the end of tension in Figures 9-10 and Figure 11 respectively, mean results are listed for each ply in Table 1 and Table 2.

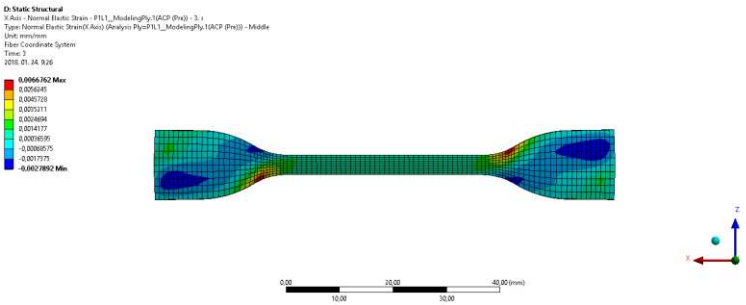

Figure 9. Strain in material direction 1, ply1

Strains in material direction 1 (yarn direction) are noticeably low (Figure 9) due to the high modulus of elasticity in material direction1, E_1= 1345 MPa.

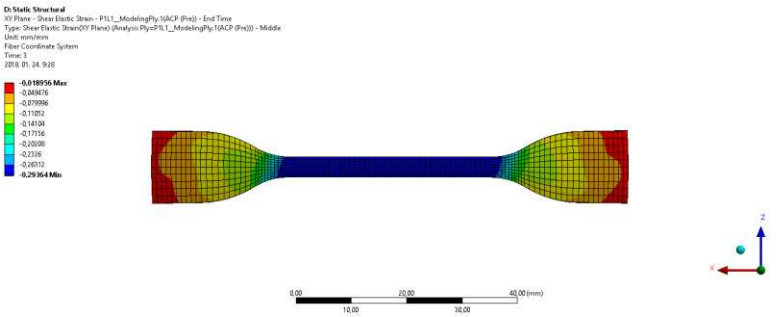

Figure 10. Strain in plane 12, ply1

Figure 10 shows strains in plane 12 in ply1. This component is the most significant in magnitude (Table 1) because the load is off-axis to the yarns, which induces significant shear stresses (Table 2). Because of relatively low shear moduli, high shear strains arise. The absolute value of shear strains is identical for every reinforcement ply, shear strains in adjacent plies have opposite signs due to the symmetric layup. Strains in material direction 2 have the same distribution as shear strains in plane 12. According to Table 1, strain components are distributed equally among plies.

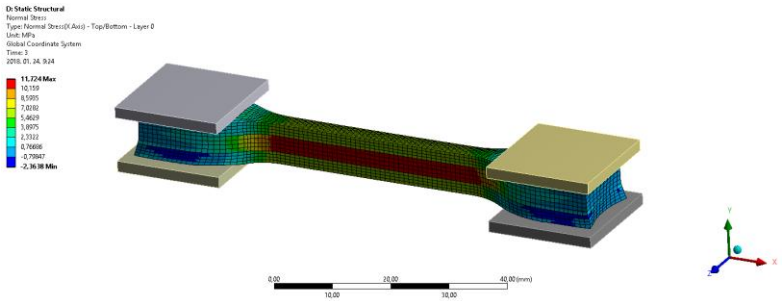

Figure 11. Stress in global X direction at a displacement of 11.7 mm

Highest longitudinal stress values arise in reinforcement layers (Figure 11), whereas approximately half the maximum values arise in rubber liners. This justifies that principally; reinforcement plies bear the load exerted on specimen. Stress components of standard test specimen in material direction 1, material direction 2 and in plane 12 have the same distribution as their strain counterparts.

Table 1. Maximum strains in reinforcement plies in the middle range in the vertical midplane YZ

ply no.	$\varepsilon_{1,\,max}$ ***[-]***	$\varepsilon_{2,\,max}$ ***[-]***	$\gamma_{12,\,max}$ ***[-]***
1	0.0013	0.1181	-0.2936
2	0.0021	0.111	0.2989
3	0.0021	0.1116	-0.3014
4	0.0013	0.1223	0.3003

Table 2. Maximum stresses in reinforcement plies in the middle range in the vertical midplane YZ

ply no.	$\sigma_{x,\,max}$ ***[MPa]***	$\sigma_{1,\,max}$ ***[MPa]***	$\sigma_{2,\,max}$ ***[MPa]***	$\tau_{12,\,max}$ ***[MPa]***
1	11.1	4.15	6.88	-5.63
2	11.49	5.19	6.42	5.73
3	11.61	5.15	6.47	-5.78
4	11.52	4.10	7.23	5.75

4. Uniaxial tension of hose piece at -40°C

4.1. Tensile test experiment of hose piece at 40°C

A 150 mm long hose piece has been subjected to uniaxial tension to a displacement of 35 mm. Cross-section of the hose piece specimen can be seen in Figure 1. Tension has been performed with the help of two steel plugs installed into the hose by pipe clamps and by bonding them to the inner liner of the hose. The hose piece has been put into a climate chamber, whose temperature had been set to -40°C (Figure 12).

Hose piece has been pulled with a tensile speed of 5 mm/min and a pre-load of 5 N.

Figure 12. Hose piece specimen at -40 °C, placed in climate chamber

4.2. FE simulation of uniaxial tension of hose piece at -40°C

Geometry of the FE model is identical to that of the experiment. Steel plugs utilized for tension are modeled as rigid bodies.

4.2.1. Connections

Reinforcement plies are in bonded contact with outer and inner rubber liners. The rigid plugs are also bonded to the inner lateral surface of the hose.

4.2.2. Loads, boundary conditions

In the first time step, pressure of 1.5 MPa, representing pipe clamps, is applied to sections of the outer side surface of the hose depicted in Figure 13.
In the second time step, a prescribed displacement of 35 mm is applied to the right end of the right plug. In the meantime, left end of the left plug is fixed.

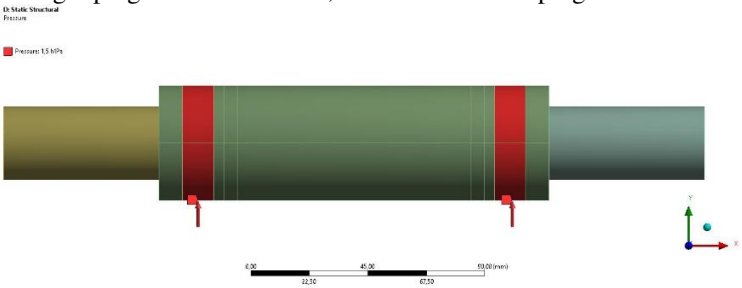

Figure 13. Pressure representing pipe clamps, 1.5 MPa

4.2.3. Material properties

Material properties of reinforcement plies and rubber liners are described in detail in Chapter 2.2.

4.3. Comparison of FE simulation and test experiment results

FE simulation and test experiment results at -40°C (Figure 16) show good agreement in the entire range of uniaxial tension.

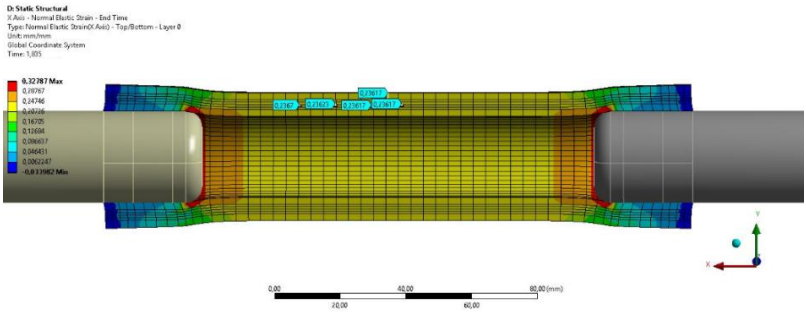

Figure 14. Strain in global X direction

Maximal strain arising in hose piece in the middle range between the steel plugs is 0.23 at a displacement of 30 mm (Figure 14), which is considered significant.

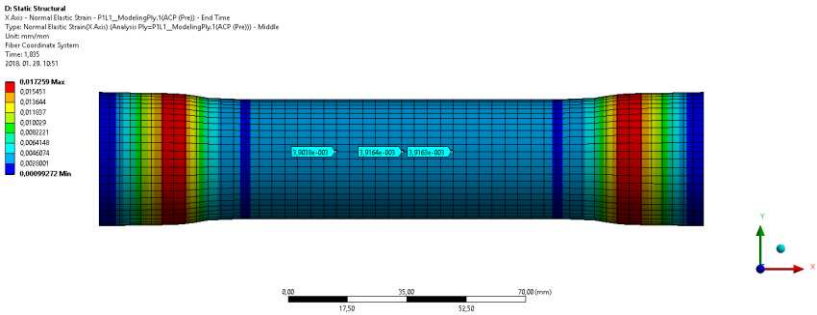

Figure 15. Strain in material direction 1, ply1

Strain in material direction 1 in yarn coordinate system can be observed in Figure 15. These strain values tend to be much lower than strains in material direction 1 due to high modulus of elasticity E_1.

Shear strain in plane 12, having the same distribution as strain in material direction 1 has a predominant role in the structural behavior of hose piece under tension because of the load being off-axis to the yarn direction and shear moduli being relatively low. Normal strain in material direction 2, having the same distribution as shear strain in plane 12, is also considerably significant being the other strain component into which global longitudinal strain is transformed. Strains are almost equally distributed along reinforcement plies.

Stress components of hose piece in material direction 1, material direction 2 and in plane 12 have the same distribution as their strain counterparts.

Maximum strain and stress results for each reinforcement ply in the middle range of the specimen between grips are presented in Table 3 and Table 4 respectively. Results are listed at a displacement of 30 mm, therefore results can be compared to results at room temperature. Table 3 and 4 also contains results of FE simulation of hose piece at room temperature.

Table 3. Maximum strains in each reinforcement ply in the middle range at -40°C in vertical midplane YZ

ply no.	$\varepsilon_{x,\,max}$ ***[-]***	$\varepsilon_{1,\,max}$ ***[-]***	$\varepsilon_{2,\,max}$ ***[-]***	$\gamma_{12,\,max}$ ***[-]***
1	0.2417 (0.2423)	0.0039 (0.0026)	0.1251 (0.1251)	-0.3398 (-0.3362)
2	0.242 (0.2437)	0.0035 (0.0018)	0.1245 (0.1245)	0.3356 (0.3406)
3	0.2447 (0.2464)	0.0026 (0.0012)	0.1252 (0.1254)	-0.3405 (-0.3464)
4	0.2469 (0.2484)	0.0029 (0.0014)	0.1279 (0.1261)	0.3452 (0.3508)

Table 4 Maximum stresses in each reinforcement ply at -40°C in vertical midplane YZ

ply no.	$\sigma_{x,\,max}$ ***[MPa]***	$\sigma_{1,\,max}$ ***[MPa]***	$\sigma_{2,\,max}$ ***[MPa]***	$\tau_{12,\,max}$ ***[MPa]***
1	13.41 (4.93)	7.88 (4.38)	7,26 (2.32)	-6.38 (-2.09)
2	12.97 (4.52)	7.72 (3.25)	7,17 (2.29)	6.43 (2.12)
3	13.61 (3.59)	3.93 (0.46)	8,42 (2.31)	-6.53 (-2.15)
4	14.62 (3.07)	1.98 (1.19)	7,38 (2.36)	6.62 (2.18)

5. Uniaxial tension of hose piece at room temperature

Arrangement of uniaxial tensile test experiment matches arrangement of the tensile test carried out at -40°C, moreover, hose piece is 150 mm long as well.
FE model differs only in the aspect of material properties from the FE model of uniaxial tension at -40°C.

Material properties of reinforcement plies at room temperature are as follows: E_1=1338 MPa, E_2=E_3=19 MPa, υ_{12}= υ_{13}=0.37, υ_{23}=0.498; G_{12}= G_{13}= G_{23}=6 MPa [13].

Material properties of rubber liners are: C_{10}= -0.4982 MPa, C_{01}= 1.523 MPa, D=0 [1/MPa] [13].

5.1. Results of uniaxial tensile test experiment and FE simulation at room temperature

FE simulation and test experiment results at room temperature show good agreement in the entire range of uniaxial tension (Figure 16).

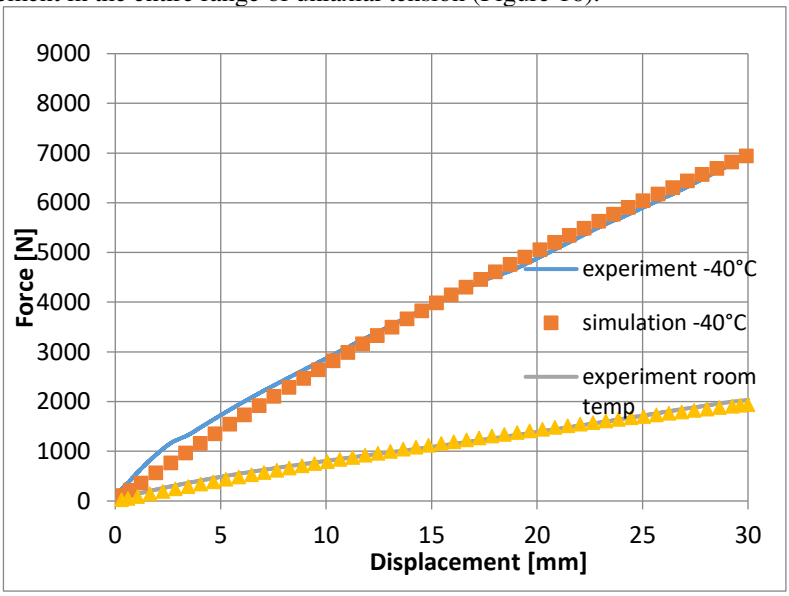

Figure 16. Force displacement curves of hose piece at -40°C and at room temperature

Proportion of the slope of force-displacement curve of hose piece at -40 °C and the slope of force-displacement curve of hose piece at room temperature is 3.4.

Maximum strain and stress results can be seen in Table 3 and Table 4 in brackets. Strain results at -40°C and at room temperature are nearly identical in the case of strain in global X direction (ε_x), strain in material direction 2 (ε_2) and strain in plane 12 (γ_{12}). Strain in material direction 1 (ε_1), strain at -40°C is twice as much as at room temperature. Stress at -40°C, in material direction 1 is 3.6 times, in material direction 2 is 3.3 times, in plane 12 is 3.3 times as much as at room temperature. The higher stresses at -40°C are attributed to the increased modulus of elasticity of rubber, stress components are nearly directly proportional to the modulus of elasticity of rubber.

6. Conclusions

Experimental and FE simulation results of standard test specimen and hose piece at -40°C and at room temperature in the entire displacement range are in good agreement with each other.

Strain values of standard test specimen at the point of rupture (displacement of 11.7 mm) at -40°C are nearly 0.9 times the strain values arising at the tension of hose piece at -40°C at a displacement of 30 mm. Stress values at -40˚C and at room temperature have the same proportion.

Strains arising in material direction 2 and in plane 12 in hose piece at a displacement of 30 mm, at -40°C have the same magnitude as at room temperature. Strain values in material direction 1, at -40°C are twice as much as values at room temperature. Strain values in material direction 2 and in plane 12 are much higher than strains in material direction 1.

Modulus of elasticity of rubber at -40°C is approximately three times the modulus of elasticity of rubber at room temperature. Stress components in reinforcement plies are approximately 3.3 times as much as those of room temperature on average. Slope of force-displacement curves of hose piece at -40°C is 3.4 times as much as the slope of that at room temperature. It can be stated that a change in moduli of elasticity (E_2, E_3) and shear moduli (G_{12}, G_{23}, G_{13}) is directly proportional to a change in the modulus of elasticity of matrix (being rubber), thus a change in stress components is directly proportional to a change in modulus of elasticity of matrix.

Acknowledgement

Technical support of Gábor Szebényi at Department of Polymer Engineering, Budapest University of Tecnology and Economics) is highly appreciated. Authors

would also like to express their gratitude to György Szabó at Department of Machine and Product Design, Budapest University of Technology and Economics for test specimen preparation.

The recent study and publication was realized within the Knorr-Bremse Scholarship Program supported by the Knorr-Bremse Rail Systems Budapest.

References

[1] C. Kaynak, O. Mat, Uniaxial fatigue behavior of filament-wound glass-fiber/epoxy composite tubes, Composites Science and Technology 61 (13) (2001) pp. 1833-1840.
doi: 10.1016/S0266-3538(01)00084-7

[2] J. H. S.Almeida Jr, M. Ribeiro, T. Volnei, S. C. Amico, Damage modeling for carbon fiber/epoxy filament wound composite tubes under radial compression, Composite Structures 160 (2017) pp. 204-210.
doi: 10.1016/j.compstruct.2016.10.036

[3] M. Carroll, F. Ellyin, D. Kujawski, A. S. Chiu, The rate-dependent behaviour of ±55° filament-wound glass-fibre/epoxy tubes under biaxial loading, Composites Science and Technology 55 (4) (1995) pp. 391-403.
doi: 10.1016/0266-3538(95)00119-0

[4] P. D. Soden, R. Kitching, P. C. Tse, Experimental failure stresses for ±55° filament wound glass fibre reinforced plastic tubes under biaxial loads, Composites, 20 (2) (1989) pp.125–135.
doi: 10.1016/0010-4361(89)90640-X

[5] P. Y. Manach, Mechanical behavior of fabric-reinforced elastomer straight flexible hoses, Applied and Computational Mechanics 2 (2008) pp. 291-302.

[6] L. P. Kollár, G. S. Springer, Mechanics of Composite Structures, Cambridge Univ. Press, Cambridge, 2003

[7] P. K. Dutta, Structural Fiber Composite Materials for Cold Regions, Journal of Cold Regions Engineering 2 (3) (1988) pp.124-134.
doi: 10.1061/(ASCE)0887-381X(1988)2:3(124)

[8] P. K. Dutta, D. Hui, Low-temperature and freeze-thaw durability of thick composites, Composites Part B: Engineering 27 (3–4) (1996) pp. 371-379.
doi: 10.1016/1359-8368(96)00007-8

[9] P. K. Dutta, Tensile strength of unidirectional fiber composites at low temperatures. Proceedings, Sixth Japan–U.S. Conference on Composite Materials, Technomic Publishing AG, Orlando, 1992, pp. 782–792.

[10] S. Sánchez-Sáez, T. Gómez-del Río, E. Barbero, R. Zaera, C. Navarro, Static behavior of CFRPs at low temperatures, Composites Part B: Engineering 33 (5) (2002) pp. 383-390.
doi: 10.1016/S1359-8368(02)00021-5

[11] K. K. Chawla, Composite Materials Science and Engineering, 3rd Edition, Springer, New York, London, 2009.

[12] C. C. Chamis, NASA Tech. Memo. 83320, presented at the 38th annual conference of the Society of Plastics Industry (SPI), Houston (1983).

[13] Gy. Szabó, K. Váradi, D. Felhős, Finite Element Model of a Filament-Wound Composite Tube Subjected to Uniaxial Tension, Modern Mechanical Engineering 7 (4) (2017), pp. 91-112.
doi: 10.4236/mme.2017.74007

[14] K. Battermann, R. Köhler, Elastomere Federung - Elastische Lagerungen: Grundlagen ingenieurmässiger Berechnung und Konstruktion, Ernst, Wilhelm & Sohn, Berlin, 1982.

[15] Ansys Mechanical User's Guide, Engineering Data User's Guide, Material Data, Mechanical Material Curve Fitting

[16] J. Karger-Kocsis, A. Mousa, Z. Major, N. Békési, Dry friction and sliding wear of EPDM rubbers against steel as a function of carbon black content, Wear 264 (3-4) (2008) pp. 359-367.
doi: 10.1016/j.wear.2007.03.021

Acta
Technica
Jaurinensis

Vol. 11, No. 2, pp.104-118, 2018
DOI: 10.14513/actatechjaur.v11.n2.462
Available online at acta.sze.hu

Blockchain Potential in Tilapia Supply Chain in Ghana

A. Rejeb[1]

[1] **Széchenyi István University, Department of Logistics and Forwarding**
Egyetem tér 1, 9026 Győr, Hungary
e-mail: abderrahmen.rejeb@gmail.com

Abstract: In a country like Ghana where Tilapia is the most preferred and cheapest source of animal protein, closer attention must be paid to the supply chain of such a product. This paper examines the major issues and problems in Tilapia supply chain and logistics in Ghana, and it suggests the intervention of the new and disruptive technology of blockchain. Blockchain technology can have the potential to revolutionize the supply chain of Tilapia in Ghana and bring many advantages to the flow of Tilapia from farmers till the end consumers. Besides, it highlights the role of blockchain in ensuring food safety and in rebuilding a trustful network of Tilapia distribution between producers and customers. A model of Tilapia supply chain based on blockchain technology will be exhibited and explained to provide relative solutions to supply chain management processes of Tilapia.

Keywords: Tilapia supply chain, Blockchain technology, Trust, Transparency, Decentralized system.

1. Introduction

Nowadays, supply chain management and logistics are considered as potent drivers of economic growth. Although firms now deal with an uncountable number of suppliers, outsourced service providers, logistic distributors, and customers, there is still ambiguity of how, when and where these products were originated, produced and used through the life cycle [1]. Similarly, the journey of products is still in every scenario unseen and beyond the supply chain partners' possession. In this context, Tilapia supply chain in Ghana represents the best frame of supply chain complexity, information asymmetry, and many other issues.

Given that fishes constitute 60 % of the protein intake in Ghana and have the potential to achieve food sufficiency, poverty alleviation and economic growth [2], the supply chain of Tilapia still knows many problems that stand against its competitiveness and profitability. In this respect, it is riddled with inefficiency since they rely heavily on paperwork, manual processes and huge numbers of people to perform a specific business transaction. In connection with inefficiency, the traditional organizational structure of aquaculture tends to drag down the supply chain through the silo mentality, wherein the inwardly focused organizational units pay insufficient attention to the external relationships and create a disjointed, disconnected and detrimental way of working [3]. Thus, there is prevention for any interaction between members of supply chain and barriers that clog the information flow between them.

Complexity is a key managerial issue that supply chain managers should address [4]. The today's immense challenges force companies to have a broad insight into products throughout the chain. It is imperative to revise the process of supply chain again and to integrate more than ever the involved partners. Hence, how companies could achieve sustainable and high performing supply chains remains the backbone question. This is neither manifested superficially by the expansion of the business nor by developing projects which are more concerned with the increased production of fish. The production of more Tilapia does not necessarily imply the profitability of farming businesses in Ghana. However, through the commitment to cope with the disruptive growth and new technologies, the profitability will increase in a sustainable manner for all value chain actors in the farmed Tilapia sector [2] [5].

Disruptive innovation is a powerful tool that taps new markets, leading to a new structure of supply chains, partners and new ways of collaboration across the network [6]. These new technologies change competition entirely by altering the performance metrics firms use to gain their competitive advantage. In this context, blockchain technology has been introduced as a breakthrough with high appreciation to its enormous potential in many fields [7].

Blockchain technology appeared firstly to support the new forms of digital currency Bitcoin in 2008. Nevertheless, it has many applications nowadays and it constitutes new foundation for a transaction in our increasingly digital society. In fact, blockchains have been deployed in reinventing currency, finance, economics, government affairs, legal services, healthcare and an unlimited number of other fields [8]. For simplicity, blockchain technology is the new pillar of distributed ledgers which trace chronologically the chain of "blocks" and each block contains a record of valid network activity since the last block was added to the chain [9]. The core principle of this new groundbreaking innovation is the decentralization of

transaction handling between industries and businesses. That is to say, there is a distributed database, replicate across many locations and operated jointly by a collective [10]. Also, researches and articles used to frame the exact meaning of blockchains are mainly periodicals since the concept is still new and at its infancy phase. The original work and application of blockchain technology has been introduced by the Japanese inventor and founder of Bitcoin Satoshi Nakamoto. Then, the same technology has been employed and affiliated to apply smart contacts and other business applications in the industry to optimize the company's operations and maximize therefore its bottom line.

This research paper will begin by introducing the literature review on the major issues in Tilapia supply chain management and logistics in Ghana. The next part will illustrate the flow diagram of the Tilapia supply chain and introduce the blockhain framework in Tilapia industry. Then, we will evaluate the contributions of blockchain adoption in Tilapia industry and how this technology will bring solutions to the problems inherited from the current supply chain model. A discussion part will be outlined base on the role of blockchain in improving customers' trust in the authenticity of supplied Tilapia and the infrastructure required to adopt this technology in Ghana. Finally, we will make a brief conclusion for the paper.

2. Literature Review

Fish and fisheries products represent one of the most traded commodities in the world food sector, accounted for 78% of seafood products traded at a global scale [11]. In this context, the Tilapia aquaculture industry experienced fast growth and it is spread throughout all continents. Tilapia is farmed in more than 80 countries and the production methods emanate from the artisanal to intensive operation [12].

Since the Food and Agriculture Organization reported rapid progress made by Sub-Saharan African countries, namely Nigeria, Uganda, Kenya, Zambia [13], the growth in aquaculture production in Ghana remains the most remarkable one. The production was estimated 26000 tons in 2012 [13]. Ghana is seen as the most capable Sub-Saharan African country to increase importantly its fish production. The reasons that put Ghana on the pedestal for this exponential growth are the development of a national aquaculture strategic framework [14], the effective policy of the national fisheries [11] , and the initiation of national aquaculture development plan that aims to increase the production from 10200 to 100000 tons between 2010 and 2016 [11]. Tilapia aquaculture production followed the current growth trend and recorded a growth of 28000 tons between 2006 to 2013 [11]. The production growth of other species has not reached the cadence of Tilapia aquaculture.

Although Ghana makes great strides in Tilapia industry, there are still persistent problems in the supply chain and logistics of such commodity. Fish farmers are unable to produce Tilapia at competitive costs on the international market [15].

Besides, the Tilapia supply chain in Ghana is characterized by its high complexity and it is fragmented into many activities, from the upstream to the downstream supply chain partners and the multitude of short chains [13].

Given that Tilapia supply chain in Ghana splits between the artisanal and the modern urban-biased (i.e., it is one among different types of the farmed Tilapia) and that there is an increased sense of better traceability in terms of products and profit flow through the modern urban-biased chain [13] because farmers are the owner of distribution or sales points, this could not deny that a gap of transparency may occur between the partners of supply chain. Besides, the aquaculture of Tilapia in Ghana is dominated by many smallholder fish farmers who have weak connections between them and their aquaculture input suppliers [5]. This weak linkage between the different actors in Tilapia value chain makes many of Tilapia farmers unable to be competitive and have strong value chain network.

Many traders and partners do not differentiate between the farmed and wild Tilapia and there is limited distinction in the marketing of wild and farmed Tilapia, and the two often share the same marketing chain [16]. Also, the buyers of Tilapia do not possess any means to follow up and evaluate the quality of Tilapia they buy from producers and farmers. The small-scale pond farmers find feeds at very high and sometimes unaffordable prices. Besides, the number of cage farmers who use consistently commercial feeds is limited due to capital constraints [5]. Alternatively, they resort to feeding source like cocoa pod husk, palm kernel cake to compound their own feed on-farm. Although they are proven to be viable, these ingredients are not produced under the strict bio-secure condition, and this subsequently affects the quality of Tilapia. Consequently, this may also give a room for quality issues, lack of trustfulness in products, and product safety risks.

The typical Tilapia supply chain in Ghana includes a vast majority of fish farmers who mostly sell their harvest to wholesalers or retailers and the retailers in return sell to the final consumers. Among the major institutions and interveners in the supply chain to support Tilapia trade operations are the fisheries commissions, Ghana Standards Authority, and Food and Drugs authority. The certification, traceability, and enforcement of sanitary conditions are the main services rendered by these institutions. Despite the presence of these regulatory bodies dedicated for fish farming control, consumers' concerns are increasing about the health implications of Tilapia due to pollution and the use of chemicals in the storage and conservation of Tilapia under unstable electricity supply conditions [17]. Therefore, Tilapia supply chain plays a major role in providing a rich source of

nutrition to Ghanaians. Proper supply chain management and building transparent value network are essential for production efficiency, processing, distribution and retailing of Tilapia that meet customer's expectations in terms of quality and sanitary conditions compliance.

3. Tilapia Supply Chain and Blockchain Technology

3.1. The Traditional Tilapia supply chain

The Tilapia supply chain follows the multi-stage supply chain system which consists of the following various actors: input suppliers, farmers, Tilapia processors, traders, retailers, institutional buyers, and final consumers. Figure 1 describes in detail the different partners of the supply chain and their roles. Input suppliers start the upstream flow in the chain. Their main role is to provide farmers with the raw materials. They consist mainly of cage and pond constructors, fingerlings suppliers, feed suppliers, and nets fishing. In addition, farmers are classified into two categories Pond Farmers and Cage grow-out Farmers. Their farmed Tilapia goes through the processors which are central to the value chain because they deal with all partners in the chain. The processors of Tilapia are predominately women [5] who provide the service of gutting and scaling the fish to traders, institutional buyers, and consumers at the points of sale. The interaction between the processors, traders and institutional buyers (e.g., restaurants, hotels) is direct since those actors do often outsource the service with bulk or large quantity of Tilapia to be processed at either distribution points or sales outlets. Traders consist of wholesalers, distributors, and retailers. Wholesalers are the only actors who are in direct connection with the farmers and they supply both distributors and retailers. Retailers can also be either provided by distributors in relatively small quantities or by wholesalers in more significant quantities. Final consumers buy Tilapia from retailers' sales point and at restaurants, hotels.

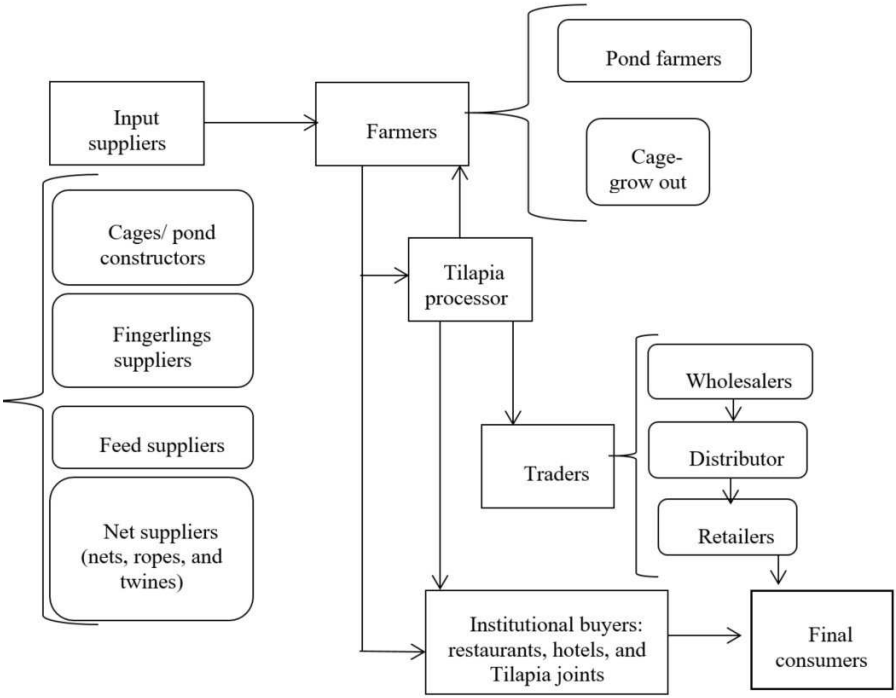

Figure 1. Tilapia Supply Chain in Ghana

3.2. Conceptual Framework of Blockchain-based Model

"*The blockchain is an exchange network for moving transactions, value, assets between peers, without the assistance of intermediaries*." [18]. It is also defined as the network of exchange and moving of value between the interested parties in the business. Besides, blockchain can be also described as the platform whereby peers or partners exchange values using transactions without the need for a central trusted arbitrator [7]. The business of blockchain encompasses the exchange of money, the flow of information and the effective allocation of resources that were enabled by money in the human and corporate level of the economy [19]. In actuality, some of the most promising non-finance applications are expected to involve those in the supply chain, power and food/ agriculture [20]. In this section, we will discuss the integration of blockchain technology in Tilapia supply chain.

So, all supply chain partners mentioned previously should register themselves in the peer-to-peer network and match their identities and digital profiles in back-end database which maintains an openly distributed ledger that can be inspected at any time and from any location [18]. After registration, each user (i.e., node) will be provided with a public and private cryptographic key. The public key serves to identify the user within the system and the private key can be used for authentication when interacting in the network. The different phases included in the value chain are: Procurements, Farming, Processing, Distributing and Retailing.

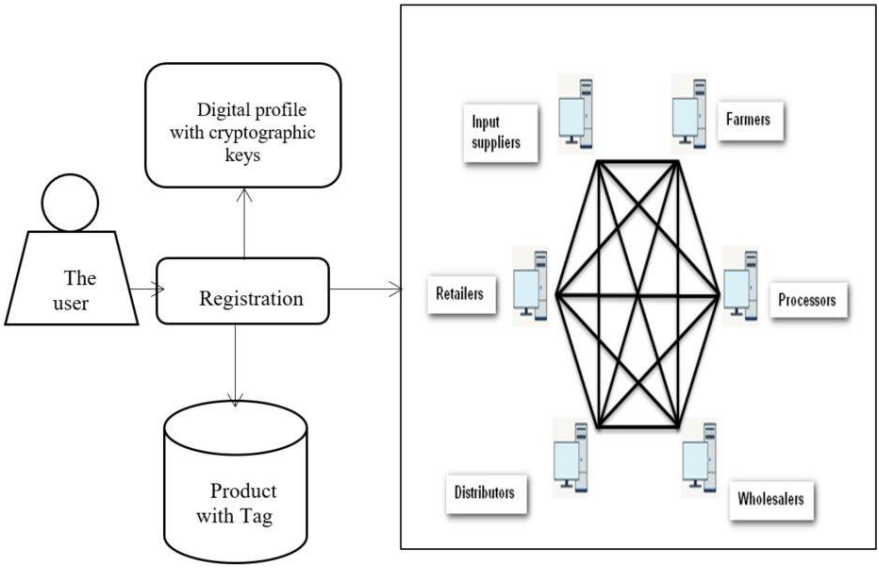

Figure 2. Conceptual framework of Tilapia blockchain (adapted from Tian 2016)

4. Evaluation of Blockchain in Tilapia Supply Chain

4.1. Procurement

At procurement stage, Farmers will get the raw materials which consist of fingerlings, hatcheries and feed supplies. The input suppliers may register under the blockchain network and a digital profile of fingerlings is updated in the distributed ledger by providing essential information about the fingerlings (e.g., the hatcheries' environment, the growth condition, information related to their feed). The implementation of blockchain in this phase will increase the quality of

fingerlings and the control over the climatic changes on hatchability of fish eggs. The challenges encountered by African farmers in general and Ghanaians in particular regarding product quality [17] could be effectively eliminated with the introduction of blockchain instead of opting for the self-production of fingerlings.

4.2. Farming

The harvested Tilapias are packaged in corrugated cardboard boxes and labeled with RFID Tag, and then each fish box will be entered into the blockchain with a digital profile. Many answers to questions regarding the system will be provided through the blockchain such as the characteristics of the harvested Tilapia, their sizes, their weights, the harvesting intervals of fish, and even the staffs responsible for their harvesting and packaging. Besides, the raising of Tilapia becomes so transparent under blockchain use since the downstream supply chain partners can figure out the quality of Tilapia feeds, the temperature, the water salinity, the oxygen levels, the volumes of water, and the stocking density of tilapia. After that, a business transaction is initiated between the farmers and the traders or the institutional buyers, where the products are exchanged after signing a digital contract (smart contract) which is resided within the blockchain in order to execute a required function when certain conditions are met (e.g. the release of funds, the transfer of information, and the purchase of Tilapia...). Consequently, the business transaction becomes automated and it crosses beyond the boundaries of the farming companies in a secure and decentralized manner. For instance, to counter the risks attributed to the shipment of Tilapia to customers, a smart contract can be the solution to ensure that the payment by the customers will be only released if the shipping company confirms the delivery of Tilapia in appropriate conditions.

4.3. Processing

The actual processing activities raise many questions relative to the adequacy of food safety knowledge [5], and the growing mandatory regulations are not enough to ensure food safety. In blockchain model, one food safety inspector can evaluate the processing facility and enter the information regarding the gutting and scaling of Tilapia, the cleanness of the processing environment, and the use of stainless tables and equipment. During the processing, tags of Tilapia unit loads may be destroyed, but their digital profiles will be updated throughout the blockchain system and new tags can be attached to the packages of processed fishes. Thus, this helps to ensure the compliance of processing operations to the necessary sanitary requirements.

4.4. Distribution

After receiving the Tilapia from processors, the information of Tilapia warehousing and storage will be continuously updated in the system. This can be achieved easily through the use of Internet of Things (IoT) equipment such as wireless sensors and monitoring devices which ensure the real-time storage information of the product (i.e., the quantity, the temperature, the humidity) [21]. Therefore, this helps managers to better track storage and make judgmental decisions relative to the release of storage in case of risks of spoilage and perishability.

The distribution process under blockchain framework entails to safety in the transportation of Tilapia. This is demonstrated by the use of vehicles equipped with a safety system which controls the temperature and the humidity in the different areas in the refrigerated containers. This enables possibilities to track real time environmental data of Tilapia and the system can be easily implemented and the integration of IoT equipment is affordable. For instance, GPS system helps to position refrigerated trucks from remote distribution centers and identifies the optimal routes to short delivery time in a way to preserve the freshness of Tilapia.

4.5. Retailing

After receiving Tilapia, all retailers maintain the full information of the flow of the product in the supply chain. The traceability of the products can be achieved through the details stored in its digital profile on the blockchain. Any person registered in the blockchain network could figure out the freshness of stored Tilapia and their shelf life in a real-time manner. Consequently, blockchain yields to shift away from the centralized tilapia supply chain to a new decentralized system which eradicates trust problems, such as frauds, tampering and falsifying product information. Furthermore, all supply chain partners are informed with the permanent history of the product and operate in a common platform which promotes more openness, transparency, reliability and security.

5. Blockchain- Based Supply Chain: Tilapia Authenticity and Infrastructure

5.1. Blockchain and Product Originality

Since the traceability system assumed in this paper is based on the use of RFID tags to store information in the different stages of the supply chain, the manual retrieval and storage of this information in the central database pose a problem. This is manifested by the possibility of reproducing or forging information at any

time [22]. Similarly, it is difficult to identify counterfeit products accompanied by misleading provenance histories. However, blockchain technology helps to ensure the authenticity and provenance of Tilapia through an effective trace-back capability. In fact, the customer can figure out the complete data and related information by entering the digital identifier (ID) in the blockchain system. When the ID is entered, the customer in the supply chain will be provided by all related information and data from the retailers to the farmers. Given that the details of sold Tilapia are also recorded in the blockchain, it is not possible to sell the same item twice. Consequently, the blockchain system prevents any fraudulent actions related to the intentional fish mislabeling and species substitutions. Besides, fish traceability is key to fighting fish fraud, enforcing the safety regulations and ensuring high standards of sustainable fisheries management [23]. In this respect, blockchain will provide a unique digital product memory for not only the finished processed Tilapia but also for the ingredients, the raw materials, and all the quality certifications and data used in the entire supply chain. Thus, it is evident that by assigning blockchain technology which is resistant to falsification, immutable, and traceable, the platform enhancement is ensured by a move toward genuine product originality assurance that meets customers' expectations.

In addition, to solve the problem of RFID tags' information interrogating and cloning while the products reach the end of supply chain and are displayed in retail stores, Toyoda et al. proposed a novel Product Ownership Management System (POMS) [24] which makes the efforts of counterfeiters to clone genuine tags redundant since they cannot prove the possession of products on this system. In fact, the concept of proving "the possession of products" and designing POMS helps to manage and track the possession of Tilapia from their input suppliers (i.e., when they are fingerlings) to the current owners (i.e., they are assumed to be retailers). With the application of this scheme, any potential counterfeits may be detected if a party cannot prove the possession of claimed products. Their proposed system is built upon the requirements of having; only the legitimate manufacturers' role to claim the initial ownership (origin) of products, each manufacturer can declare their own products, the events "Shipped" and "Received" can be separated, and a manufacturer must give some incentives to each party who follows the POMS protocol [24]. The overall objective of their proposed solution in supply chain applications of the blockchain technology is the proof of origin [25] which helps in turn to increase customers' trust in products' originality.

To sum up, the traceability of provenance under blockchain system helps to assure that no individual entity or actor can corrupt the chain of custody and hence the final consumers will have more trust in the supplied Tilapia.

5.2. Blockchain Infrastructure and Challenges in Ghana:

Several blockchain projects were underway in so many countries, and the speed of expansion of government-led blockchain projects is astonishing at the global scale [26]. Moreover, to face the problems related to land registry in Ghana and the corruption that creates obstacles for both citizens and foreign investors in all kinds of real estate and business dealings, Bitland was introduced in 2013 as an experimental platform using blockchain technology to bridge the gap between the government and the undocumented areas for land registry and title services [27]. Another startup called Benben was created for the same purpose. Therefore, Ghana has benefited from existing tech hubs and networks to adopt blockchain technology and thus have a fertile innovation ecosystem that could enhance its local development [28] and extend to other fields such as supply chains and logistics.

The concentration of food production in developing countries involves many challenges in the supply chains since there are high corruption levels and insufficient environmental, social and economic regulatory frameworks [29]. Thus, a decentralized platform based on the blockchain technology is an interesting option for these countries. For blockchain to be implemented in Tilapia supply chain in Ghana, the engagement across the whole supply chain is required. In other words, the input suppliers, farmers, processors, wholesalers, retailers, and other supply chain actors must be willing to adopt the technology. Besides, internet connectivity and digital literacy are required for the potential adoption of these technologies in the aquaculture sector since the most significant operational risks and challenges are mainly due to insufficient (and few) numbers of people who understand blockchain functioning [30]. Infrastructure partnerships including the government, international companies (e.g., IBM) and potential startups can work jointly to raise new solutions for current problems in Tilapia supply chain. Moreover, blockchains rely heavily on the extensive use of cryptographic tools which require the development of several kinds of infrastructure, or infostructure known as public key infrastructure [28]. This infrastructure consists of a set of roles, policies, and procedures required for securing the electronic transfer of information between the supply chain actors. Although the institutional capacities in developing countries are not enough for harnessing blockchain technology and facilitating its adoption on a sustained basis, Ghana institutions can embrace the use of blockchains by either importing know-how and expertise or using local expertise, if available, outside government [28].

Despite that fact that blockchain technology may contribute to the reduction of transaction time and costs by eliminating third-party intermediaries within the Tilapia supply chain and overhead costs for exchanging the products, the high initial implementation cost can be a deterrent for small farmers in the aquaculture

sector [30]. Additionally, the Ghanaian government may consider putting more efforts into blockchain adoption in Tilapia supply chain by a further promotion of the cultural acceptance and the shift brought by this technology in the sector of aquaculture. The government support by funding and setting the appropriate regulatory framework is necessary for the successful implementation of other extended blockchain projects.

6. Conclusion

This paper aims to present the potential benefits that blockchain technology could bring to supply chain management and logistics. As an application scenario, the case of a much-traded commodity in Ghana is chosen to demonstrate how blockchain can solve the current problems and pitfalls in the supply chain of Tilapia. This new disruptive technology is a ground-breaking innovation which emphasizes the importance of a decentralized system in improving visibility, traceability, and collaboration across the supply chain. Businesses, suppliers, retailers, and distributors get hold of events happening within the chain and monitor the quality and safety of Tilapia. In the near future, Tilapia supply chain actors may consider to invest in tracking technologies such as RFID, GPS, genetic marking and to store all the critical data gathered in this process on a blockchain to ensure transparency and traceability for aquaculture farmers, consumers and everyone in between. This research taps a new area in supply chain management since blockchain implementation in such field is still yet at its infancy stage and it provides solutions to the current customers' growing concerns about safety and quality products in food supply chain.

References

[1] S. A. Abeyratne and R. P. Monfared, Blockchain Ready Manufacturing Supply Chain Using Distributed Ledger, 2016. DOI:10.15623/ijret.2016.0509001

[2] A. R. Kaliba, S. Amisah, L. Kumah, and K. K. Quagrainie, Economic analysis of Nile tilapia production in Ghana, Q. J. Int. Agric., vol. 46, no. 2, pp. 105–117, 2007.

[3] H. Vatanpour, A. Khorramnia, and N. Forutan, Silo effect a prominence factor to decrease efficiency of pharmaceutical industry, Iran. J. Pharm. Res., vol. 12, no. SUPPL., p. 210, 2013.

[4] P. Németh and P. Foldesi, Efficient Control of Logistic Processes Using Multi-criteria Performance Measurement, Acta Tech. Jaurinensis Ser. Logist., vol. 2, no. 3, pp. 353–360, 2009.

[5] G. Anane-Taabeah, K. Quagrainie, and S. Amisah, Assessment of farmed tilapia value chain in Ghana, Aquac. Int., vol. 24, no. 4, pp. 903–919, 2016. DOI: 10.1007/s10499-015-9960-1

[6] L. Pérez, V. Dos Santos Paulino, and J. Cambra-Fierro, Taking advantage of disruptive innovation through changes in value networks: insights from the space industry," Supply Chain Manag. An Int. J., vol. 22, no. 2, pp. 97–106, 2017.
DOI: 10.1108/SCM-01-2017-0017

[7] I. Bashir, Mastering Blockchain. Packt Publishing - ebooks Account (March 17, 2017), 2017.

[8] S. Chen, R. Shi, Z. Ren, J. Yan, Y. Shi, and J. Zhang, A Blockchain-Based Supply Chain Quality Management Framework, 2017 IEEE 14th Int. Conf. E-bus. Eng., pp. 172–176, 2017.
DOI: 10.1109/ICEBE.2017.34

[9] S. Bogart and K. Rice, "The Blockchain Report: Welcome to the Internet of Value," 2015.

[10] S. Farrell and W. Mallesons, "Risks and Opportunities for Systems Using Blockchain and Smart Contracts," no. May, 2017.

[11] FAO, FAO Fisheries and Aquaculture Circular FIAA/C1130 (En) Social and economic performance of tilapia farming in africa, vol. 1130. 2017.

[12] T. B. Ana Norman-López, Is tilapia the same product worldwide or are markets segmented ?, in IIFET 2008 Vietnam Proceedings, 2008, pp. 1–12.

[13] Y. B. Ansah, Enhancing Profitability of Pond Aquaculture in Ghana through Resource Management and Environmental Best Management Practices, 2014. (Master thesis)

[14] J. K. Ofori, E. K. Abban, A. Y. Karikari, and R. E. Brummett, Production parameters and economics of small-scale tilapia cage aquaculture in the Volta

Lake, Ghana, J. Appl. Aquac., vol. 22, no. 4, pp. 337–351, 2010.
DOI: 10.1080/10454438.2010.527591

[15] E. K. Hamenoo, The role of the market in the development of aquaculture in Ghana, no. May, pp. 1–64, 2011.

[16] L. Z. B. Ndanga, K. K. Quagrainie, and J. L. Dennis, Value chain development for tilapia and catfish products: Opportunities for female participation in Kenya, vol. 1529720, p. 191, 2012.

[17] F. Milani, L. García-Bañuelos, and M. Dumas, Blockchain and business process improvement, Newsl. (October 2016), 2016.

[18] W. Mougayar, The Business Blockchain. Wiley, 2016.

[19] M. Swan, Commentary Blockchain Thinking, IEEE Technol. Soc. Mag., no. December, pp. 41–52, 2015.
DOI: 10.1109/MTS.2015.2494358

[20] N. Kshetri, 1 Blockchain's roles in meeting key supply chain management objectives, International Journal of Information Management, 2018, vol. 39, pp. 80–89.
DOI: 10.1016/j.ijinfomgt.2017.12.005

[21] A. Singh and J. T. C. Teng, Enhancing supply chain outcomes through Information Technology and Trust, Comput. Human Behav., vol. 54, pp. 290–300, 2016.
DOI: 10.1016/j.chb.2015.07.051

[22] K. Biswas, V. Muthukkumarasamy, and W. L. Tan, "Blockchain Based Wine Supply Chain Traceability System," Futur. Technol. Conf., no. December, 2017.

[23] Food and Agriculture Organization, Overview of Food Fraud in the Fisheries Sector, vol. 1165. 2018.

[24] K. Toyoda, P. Takis Mathiopoulos, I. Sasase, and T. Ohtsuki, "A Novel Blockchain-Based Product Ownership Management System (POMS) for Anti-Counterfeits in the Post Supply Chain," *IEEE Access*, vol. 5, pp. 17465–17477, 2017.

DOI: 10.1109/ACCESS.2017.2720760

[25] H. Wu, Z. Li, B. King, Z. Ben Miled, J. Wassick, and J. Tazelaar, "A distributed ledger for supply chain physical distribution visibility," *Inf.*, vol. 8, no. 4, pp. 1–18, 2017.
DOI: 10.3390/info8040137

[26] M. Jun, "Blockchain government - a next form of infrastructure for the twenty-first century," *J. Open Innov. Technol. Mark. Complex.*, vol. 4, no. 1, p. 7, 2018.
DOI: 10.1186/s40852-018-0086-3

[27] V. L. Lemieux, "Blockchain technology for recordkeeping : help or hype?," vol. 1, no. October, pp. 1–6, 2016.
DOI: 10.13140/RG.2.2.28447.56488

[28] R. Zambrano and International Development Research Centre, "Blockchain - Unpacking the disruptive potential of blockchain technology for human development," p. 85, 2017.

[29] K. M. Future, "Blockchain use cases for food traceability and control."

[30] V. Morabito, "Business Innovation Through Blockchain," *Springer*, pp. 21–40, 2017.
DOI: 10.1007/978-3-319-48478-5